Supplementary Information for

Precise synthesis of sub–3 nm platinum–based intermetallic alloy with freeze–microwave confinement strategy for hydrogen evolution reaction

Xiaoyu Hu[1,2†], Shaorou Ke[1†], Xin Li[1†], Yajing Zhao[1], Xinyu Zhu[1], Yanghong Li[1], Bozhi Yang[1], Shujie Yang[1], Yangai Liu[1], Zhaohui Huang[1], Minghao Fang[1], Hao Zhang[6], Fengkun Hao[1,3*], Weiyi Zhang[5*], Shumin Zhang[4*], Xin Min[1,7*]

[†]These authors contributed equally to this work.

[*]Corresponding author.

E-mail address: minx@cugb.edu.cn; szhang788@suda.edu.cn; zhangweiyi@sdas.org; fengkuhao2–c@my.cityu.edu.hk;

Experimental Section

Chemicals and materials

Chloroplatinic acid hexahydrate ($H_2PtCl_6·6H_2O$, AR), ferric chloride hexahydrate ($FeCl_3·6H_2O$, 98%), manganese chloride ($MnCl_2$, AR), cobalt chloride hexahydrate ($CoCl_2·6H_2O$, AR), zinc chloride ($ZnCl_2$, AR), chromium trichloride hexahydrate ($CrCl_3·6H_2O$, AR), nickel chloride hexahydrate ($NiCl_2·6H_2O$, AR) and potassium hydroxide (KOH, ⩾85.0%) were supplied by Shanghai Aladdin Biochemical Technology Co., Ltd. While the conductive carbon black Ketjen-EC-300J, Commercial 20 wt% Pt/KB and 5 wt% Nafion solutions were supplied by Shanghai Hesen Co., Ltd. The ultrapure water (⩾18.2 MΩ·cm) was purchased from Shanghai Diena Biotechnology Co., LTD. Sulfuric acid (H_2SO_4, 98%) and anhydrous ethanol (C_2H_5OH) were purchased from Beijing Chemical Reagent Ltd.

Catalyst preparation

Synthesis of T–KB and U–KB. First, 100 mg of carbon black Ketjen–EC–300J was added to 40 ml of deionized water, and the mixture was treated with an ultrasonic cell disrupter (JY92–IIN, SCIENTZ–IID, China) for 6 min with a setting of 3 s of continuous operation and an interval of 9 s (total effective operating time 90 s) to achieve homogeneous dispersion at room temperature. The uniformly mixed suspension was then transferred to a vacuum freeze dryer and freeze–dried at -60 ℃ for 24 h to form a solid ice matrix; this sample was microwaved for 30 s, and after melting, centrifugation and drying yielded T–KB. For U–KB, the uniformly mixed suspension was frozen at -60 ℃ for 24 h without microwave treatment, and after natural

melting, centrifugation and drying were performed to obtain the sample.

Synthesis of Pt_3Fe/KB–MV, $L1_2$–Pt_3Fe/KB, A1–PtFe/KB. First, 40 ml of a mixed aqueous solution of chloroplatinic acid at a concentration of 0.010 mol/L and ferric chloride at a concentration of 0.010 mol/L was prepared. Then, 100 mg of carbon black Ketjen–EC–300J was added to the aqueous solution, and the mixture was treated with an ultrasonic cell disrupter (JY92–IIN, SCIENTZ–IID, China) for 6 min, with a setting of 3 s of continuous operation and an interval of 9 s to ensure a total operating time of 90 s to ensure a homogeneous mixing of the reactants at room temperature. The mixed suspension was then transferred to a vacuum freeze dryer and freeze–dried at -60 ℃ for 24 h to form a uniform ice layer of precursor concentration. (Please note that all chemicals, solutions and ice are stored under dark conditions to avoid decomposition of H_2PtCl_6 under ambient light.) Next, the ice was microwaved in a microwave oven for 30 s. After the ice melts, Pt_3Fe/KB–MV is obtained through centrifugation and drying. The Pt_3Fe/KB–MV was annealed in an argon atmosphere for 2 h at 800 ℃ and 600 ℃ respectively (ramp rate of 2 ℃/min). The samples were cooled naturally in an argon atmosphere to get $L1_2$–Pt_3Fe/KB and A1–PtFe/KB.

Synthesis of Pt_3Fe/KB–unfrozen catalysts. The synthesis of Pt_3Fe/KB–unfrozen was similar to the synthesis of $L1_2$–Pt_3Fe/KB, except that the precursor was not frozen before microwave treatment, and the suspension after ultrasonic cell pulverization was directly subjected to microwave treatment, and other processes were the same.

Synthesis of Pt_3Fe/KB catalysts under different precursor solution concentrations. The synthesis of Pt_3Fe/KB catalysts under different precursor solution concentrations

were similar to that of $L1_2$–Pt_3Fe/KB, expect that the concentrations of both chloroplatinic acid and ferric chloride in the 40 mL mixed aqueous solution were changed to 0.005 mol·L^{-1} and 0.015 mol·L^{-1}, respectively, to obtain Pt_3Fe/KB–5 and Pt_3Fe/KB–15.

Synthesis of Pt_3Fe/KB catalysts with different microwave times. The synthesis of Pt_3Fe/KB catalysts with different microwave times was similar to that of $L1_2$–Pt_3Fe/KB, except that the microwave time was changed to 0 s, 15 s and 45 s, respectively, to obtain Pt_3Fe/KB–no microwave, Pt_3Fe/KB–15 s and Pt_3Fe/KB–45 s.

Synthesis of catalysts with different annealing temperatures. The synthesis of Pt_3Fe/KB catalysts with different annealing temperatures was similar to that of $L1_2$–Pt_3Fe/KB, except that the annealing temperature was changed to 500 ℃, 700 ℃ and 900 ℃, to obtain Pt_3Fe/KB–500, Pt_3Fe/KB–700 and Pt_3Fe/KB–900, respectively.

Synthesis of catalysts with different metal ratios. The synthesis of catalysts with different metal ratios (Pt_3Fe/KB–1:3, Pt/KB, Pt_3Fe/KB–3:1, Fe/KB) was similar to that of $L1_2$–Pt_3Fe/KB, except that the concentrations of chloroplatinic acid and ferric chloride were adjusted to change the metal ratio. For Pt_3Fe/KB–1:3, the mixture contained 0.010 mol L^{-1} chloroplatinic acid and 0.03 mol L^{-1} ferric chloride. For Pt/KB, it contained 0.010 mol L^{-1} chloroplatinic acid with no ferric chloride. For Pt_3Fe/KB–3:1, it contained 0.03 mol L^{-1} chloroplatinic acid and 0.01 mol L^{-1} ferric chloride. For Fe/KB, it contained 0.01 mol L^{-1} ferric chloride with no chloroplatinic acid.

Synthesis of Pt_3Cr/KB, Pt_3Mn/KB, Pt_3Co/KB, Pt_3Ni/KB, Pt_3Cu/KB and Pt_3Zn/KB. The synthesis of these catalysts was similar to that of $L1_2$–Pt_3Fe/KB, except that the

metal chloride precursor (MCl_x) was changed to chromium trichloride hexahydrate, manganese chloride, cobalt chloride hexahydrate, nickel chloride hexahydrate, and zinc chloride, to obtain Pt_3Cr/KB, Pt_3Mn/KB, Pt_3Co/KB, Pt_3Ni/KB and Pt_3Zn/KB, respectively.

Characterization

X-ray diffraction (XRD) analyses were conducted on a high-power X–ray diffractometer (Bruker, D8 Advance) at a scanning rate of 5°/min. Electron paramagnetic resonance (EPR) spectra were acquired using a Bruker EMXplus–6/1 spectrometer. For transmission electron microscopy (TEM) characterization, the samples were dispersed onto a copper grid coated with a thin holey carbon film. High-resolution TEM (HR–TEM) was performed on all the catalyst samples using an FEI Tecnai G2 F30 microscope. High-angle annular dark-field STEM images were acquired from a corrected FEI Titan Cubed Themis G2 microscope operating at 300 kV, equipped with an X–FEG gun and a Bruker Super–X EDX detector. Atomic resolution HAADF–STEM images were obtained on probe aberration-corrected JEOL JEM-F200F and were conducted under an operating voltage of 200 KV. The molecular structure and chemical composition were analyzed using Raman spectroscopy (Horiba LabRAM HR Evolution, Japan) in the wavenumber range of 50-4000 cm^{-1}. The Pt and Fe content in the electrocatalyst was measured via Inductively coupled plasma optical emission spectrometer (Agilent ICP–OES 5800, USA). X–ray photoelectron spectroscopy (XPS) measurements were performed using an X–ray photoelectron spectrometer (Thermo Scientific *K*–Alpha, USA). The binding energy of the C 1s peak

(284.8 eV) was used as a standard to calibrate the binding energies of other elements. X–ray Absorption Fine Structure (XAFS) measurements, which include both X–ray Absorption Fine Structure (XANES) and X–ray Absorption Near Edge Structure (EXAFS) measurements of the Pt L_3 absorption edge were conducted at the Shanghai Synchrotron Radiation Facility (SSRF, China). The obtained data was analyzed using Athena and Artemis, which are software programs available in the IFEFFIT package[1].

Electrocatalytic measurements

Three-Electrode Electrochemical Evaluation

The relevant electrochemical performance was evaluated on an electrochemical workstation (CHI 760E, Shanghai Chenhua Instrument Co., Ltd.) using a standard three electrode system. The working electrode was a sample assembled with a glassy carbon electrode (d=5 mm) and a graphite rod served as the counter electrode while the reference electrode was a Hg/HgO electrode in saturated KOH solution in the alkaline electrolyte (1.0 M KOH, pH=14) and a Ag/AgCl electrode in saturated KCl solution in the acidic electrolyte (0.5 M H_2SO_4, pH=0), respectively. Calibrate all measured potentials as reversible hydrogen electrodes (RHE) according to the following equations:

$$E_{\mathrm{RHE}} = E_{\mathrm{Ag/AgCl}} + 0.059 \times pH + 0.197$$

$$E_{\mathrm{RHE}} = E_{\mathrm{Hg/HgO}} + 0.059 \times pH + 0.098$$

LSV curves without iR correction and with 80% iR were tested, respectively. Cyclic voltammetry curves at different sweep rates (20 mV s^{-1}, 40 mV s^{-1}, 60 mV s^{-1}, 80 mV s^{-1}, 100 mV s^{-1}) were plotted in the non–Faraday potential region of the electrocatalyst

to determine the C_{dl} of the catalyst. The Tafel slope of all samples was determined using the following equation:

$$\eta = b \times log|j| + a$$

where j is the current density of the sample, where η is the overpotential at a current density of j, where b is the Tafel slope of the sample and a is the Tafel constant. Chronoamperometric testing was conducted in 0.5 M H_2SO_4 and 1.0 M KOH, running continuously for 20 h under an overpotential of 2 mV vs. RHE. The stability test of the samples was assessed by comparing the LSV test results before and after 1000 cyclic voltammetry cycles and Chronoamperometric testing for 20 hours. MA is defined as the amount of current per mass of Pt (A mg_{Pt}^{-1}). The Pt content of the catalysts was determined through ICP–OES.

Two-Electrode Overall Water Splitting (OWS) Evaluation

OWS performance was evaluated using a two-electrode configuration with glassy carbon electrodes as both the cathode and anode substrates. The working electrode preparation process was consistent with that used for the three-electrode system measurements. The cathode electrode was loaded with the $L1_2$–Pt_3Fe/KB prepared in this work as the HER active material, whereas the anode electrode was coated with commercial IrO_2 catalyst for the oxygen evolution reaction. The two as-prepared electrodes were positioned face-to-face in the electrolytic cell to avoid additional voltage loss caused by uneven contact or inconsistent distance. The corresponding polarization curves were obtained by linear sweep voltammetry (LSV) measurements from 1.2 to 2.0 V with a scan rate of 5 mV s^{-1}.

Ordering degree calculation

The ordering degree was estimated by comparing the normalized intensity of the (110) peak to the sum of the intensities of the (111) and (200) peaks between the experimental XRD patterns and standard Powder Diffraction File cards of $L1_2$–Pt_3Fe. The calculation

formula is as follows[2–4]

$$\text{Ordering degree (\%)} = \frac{\frac{S(110)}{S(111)+S(200)}}{\frac{I_{PDF}(110)}{I_{PDF}(111)+I_{PDF}(200)}} \times 100\%$$

$\frac{S(110)}{S(111)+S(200)}$ is the integrated area under (110) peak and the sum of integrated area under (111) and (200) peak of the experimental XRD pattern, respectively. $\frac{I_{PDF}(110)}{I_{PDF}(111)+I_{PDF}(200)}$ is the intensity at (110) peak and the sum of the intensity at (111) and (200) peak of the Powder Diffraction File, respectively.

DFT calculation

All the calculations were assessed using the DFT with the projector augmented plane-wave method, which was implemented in the Vienna ab initio simulation package[5]. Perdew-Burke-Ernzerhof (PBE) generalized gradient approximation was used to determine the exchange-correlation potential[6]. A cut-off energy of 450 eV was set for the plane wave. The Kohn-Sham equation was solved iteratively with an energy criterion of 10^{-5} eV. The structures were relaxed until the residual forces on the atoms decreased to $<$ 0.02 eV/Å. The Gibbs free energy change (ΔG) of each elementary reaction can be computed by the following equation: $\Delta G = \Delta E + \Delta ZPE - T\Delta S$. Where ΔE, ΔZPE, T, and ΔS are the reaction energy difference, zero-point energy change, temperature, and entropy change, respectively. The d–band electronic structure of noble metal is crucial for adsorption energy of adsorbate. The d–band center is one of the simplest models to reflect the d band, as followed:

$$\varepsilon_d = \frac{\int_{-\infty}^{+\infty} \eta_d(\varepsilon)\varepsilon d\varepsilon}{\int_{-\infty}^{+\infty} \eta_d(\varepsilon) d\varepsilon}$$

where ε is energy referring to E–Fermi, $\eta_d(\varepsilon)$ is density of states (DOS) projected onto d–states.

Figure S1. The photograph of two-electrode system for overall water splitting test.

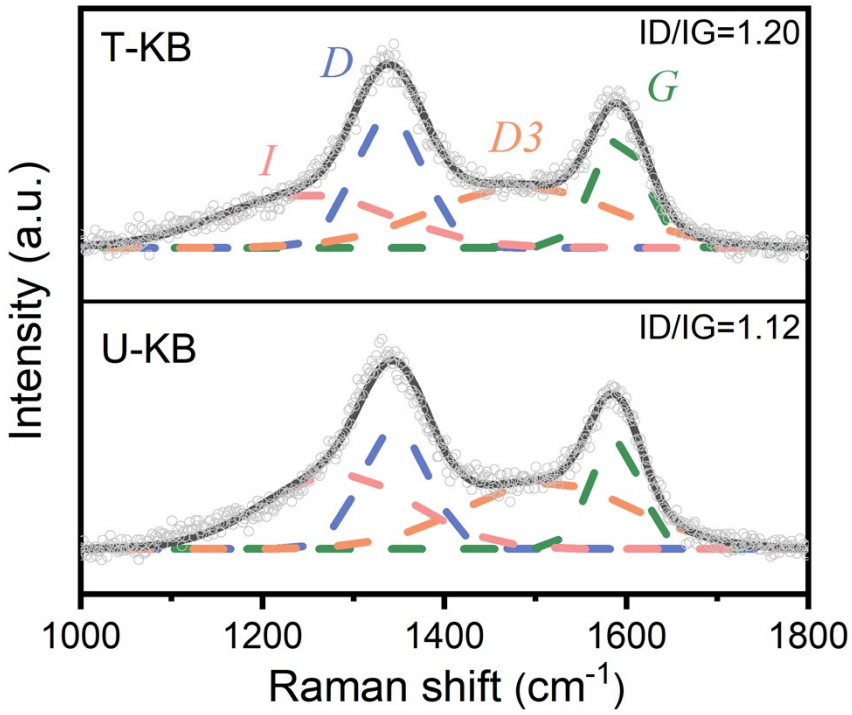

Figure S2. Raman spectra of T–KB and U–KB.

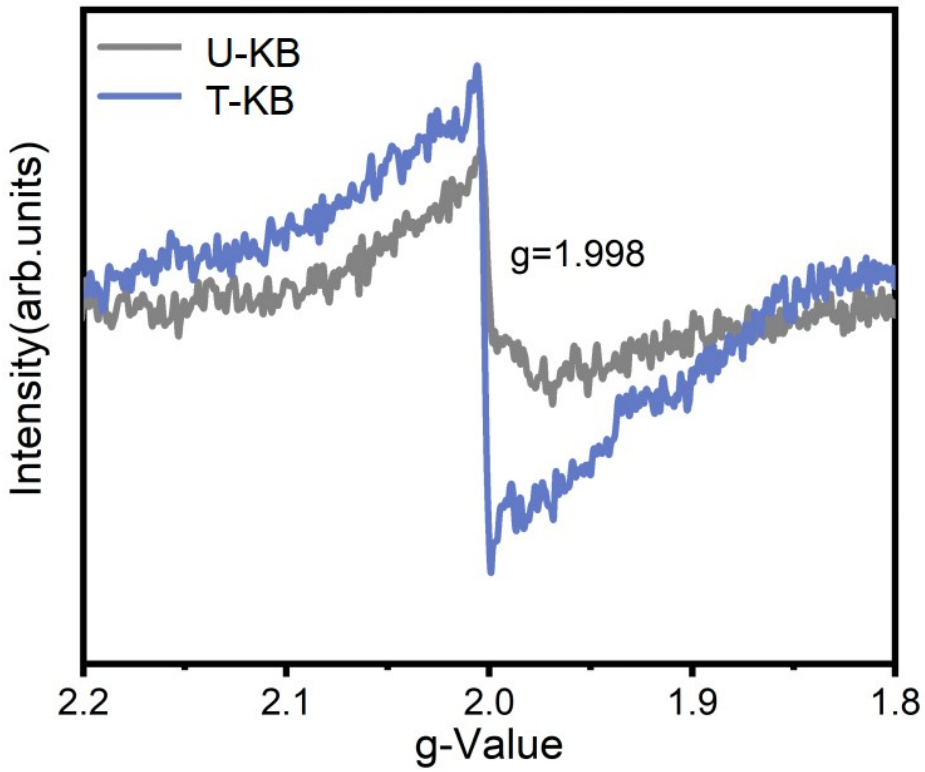

Figure S3. EPR spectra of T–KB and U–KB.

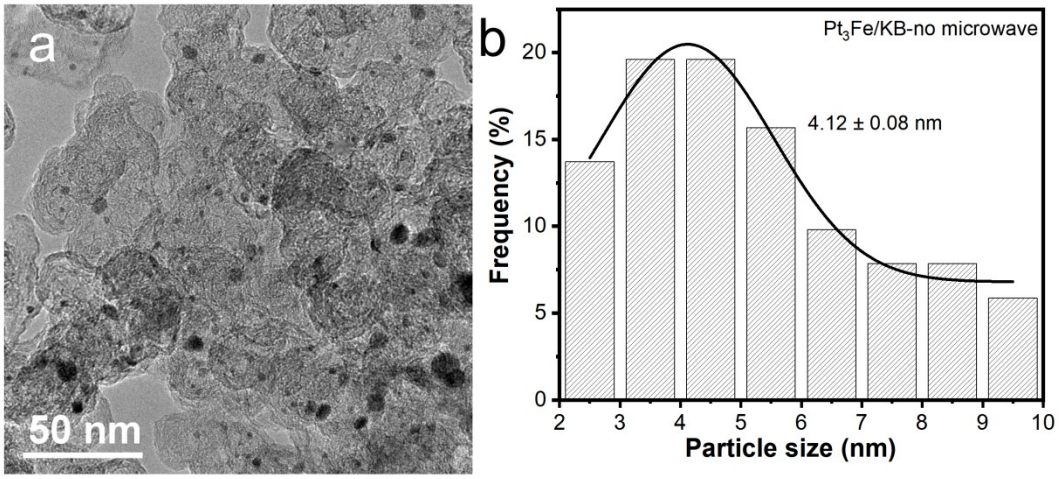

Figure S4. (a) TEM image and (b) the corresponding particle size distribution of Pt_3Fe/KB–no microwave.

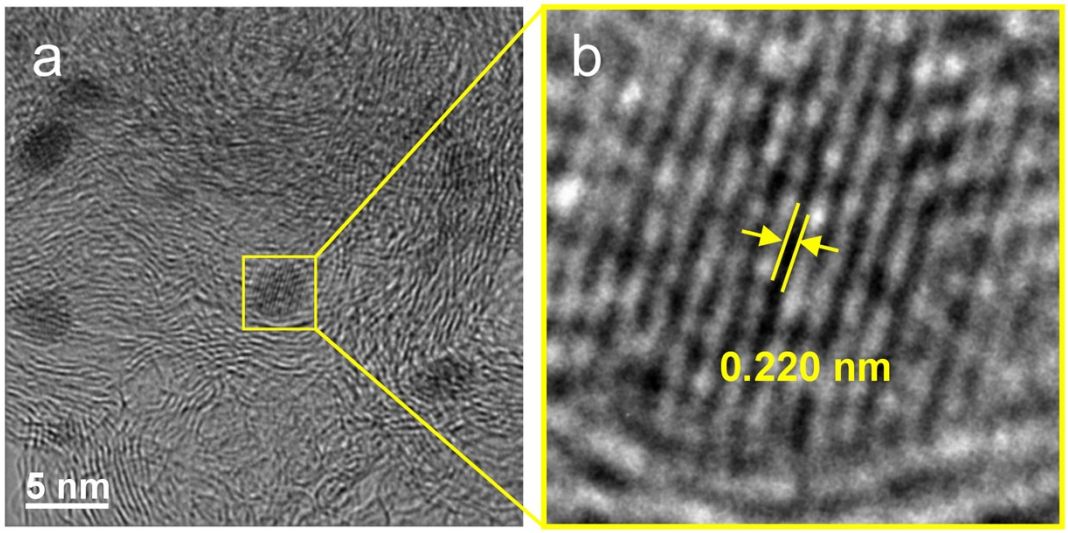

Figure S5. (a) HR–TEM image and (b) the corresponding enlarged region within the rectangular area of $L1_2$–Pt_3Fe/KB.

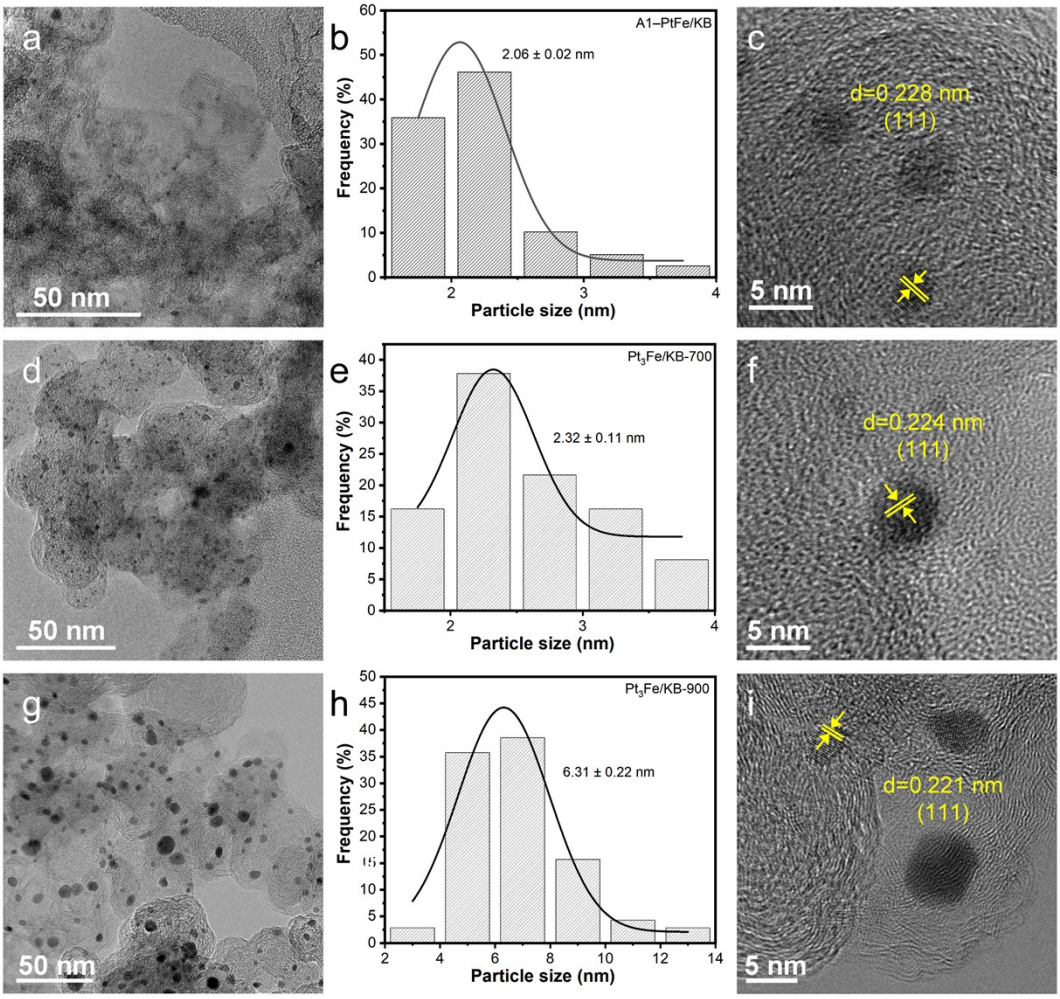

Figure S6. TEM images, the corresponding particle size distributions and HR–TEM images of (a–c) A1–PtFe/KB, (d–f) Pt_3Fe/KB–700 and (g–i) Pt_3Fe/KB–900, respectively.

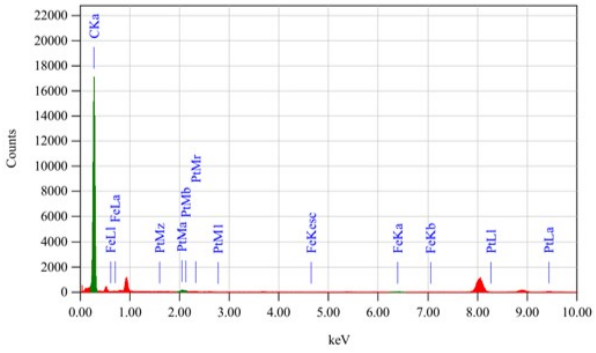

Element	Atom%
C	99.9%
Pt	2%
Fe	8%

Figure S7. EDS spectra and atomic ratios corresponding to the EDS mapping in Fig. 1d for the $L1_2$–Pt_3Fe/KB. Inset: a table showing the atomic ratios by EDS.

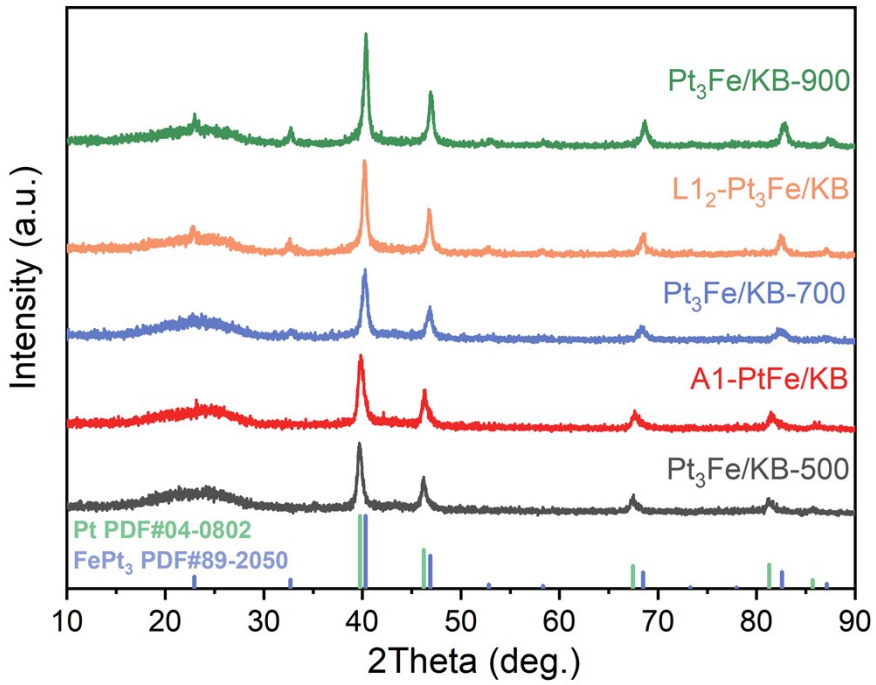

Figure S8. XRD patterns of the Pt_3Fe/KB–500, A1–PtFe/KB, Pt_3Fe/KB–700, $L1_2$–Pt_3Fe/KB and Pt_3Fe/KB–900, respectively.

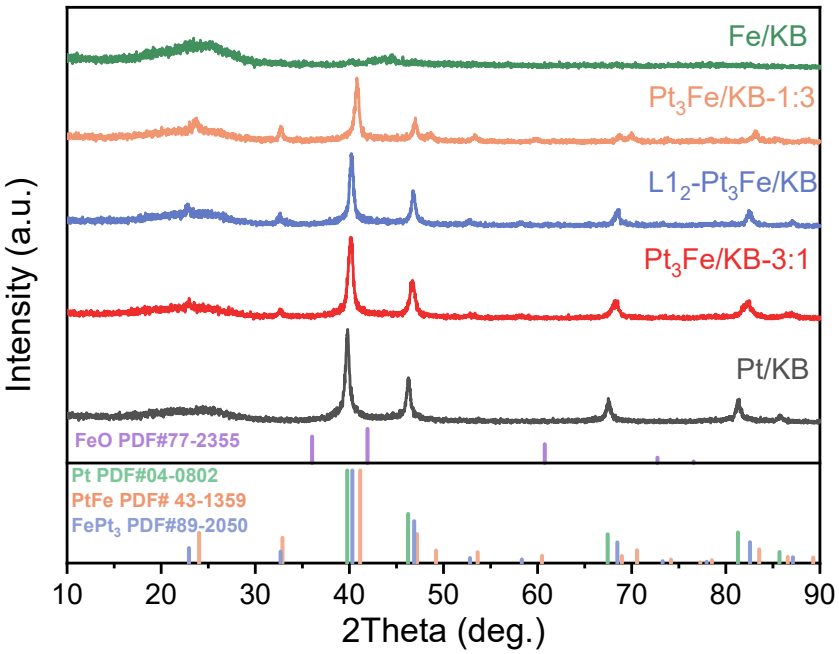

Figure S9. XRD patterns of the Pt/KB, Pt_3Fe/KB–3:1, $L1_2$–Pt_3Fe/KB, Pt_3Fe/KB–1:3 and Fe/KB, respectively.

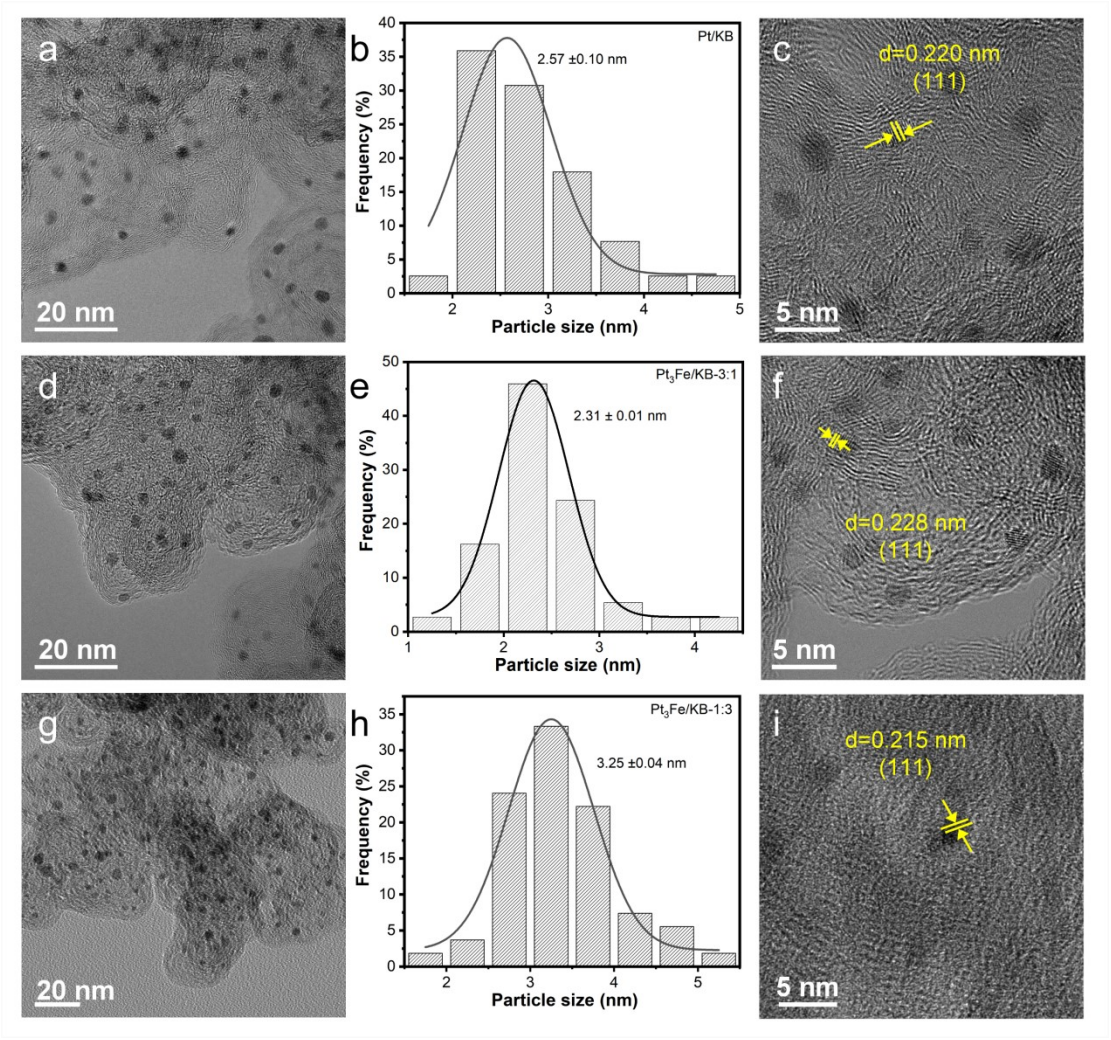

Figure S10. TEM images, the corresponding particle size distributions and HR–TEM images of (a–c) Pt/KB, (d–f) Pt_3Fe/KB–3:1 and (g–i) Pt_3Fe/KB–1:3, respectively.

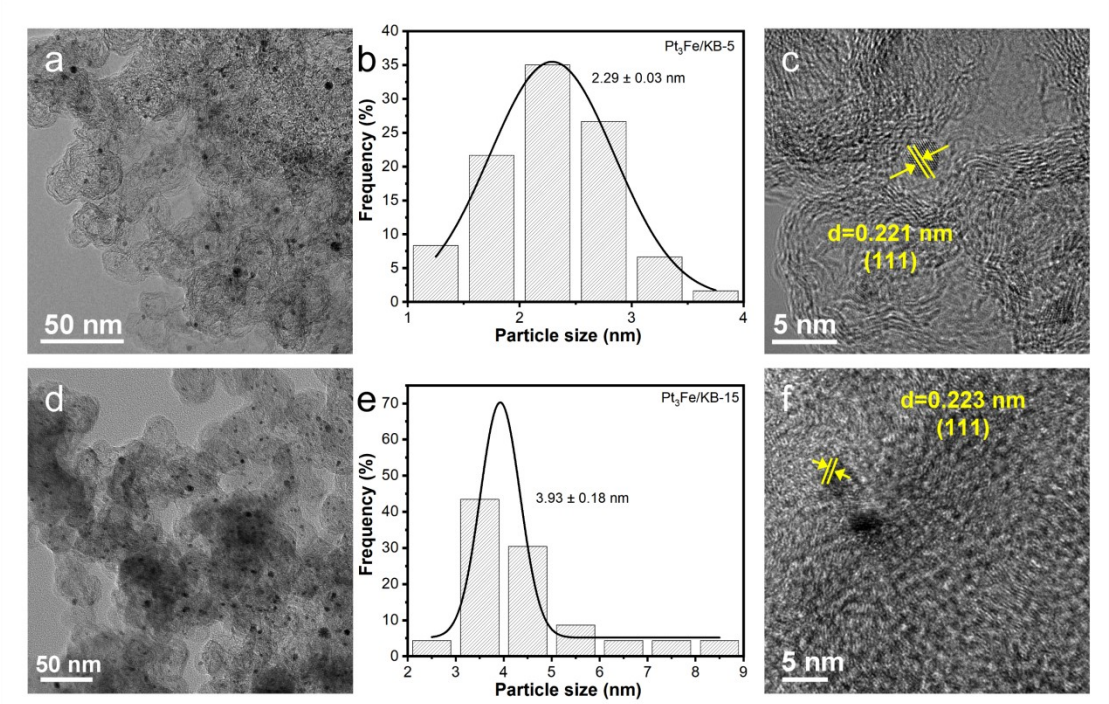

Figure S11. TEM images, the corresponding particle size distributions and HR–TEM images of (a–c) Pt_3Fe/KB–5 and (d–f) Pt_3Fe/KB–15, respectively.

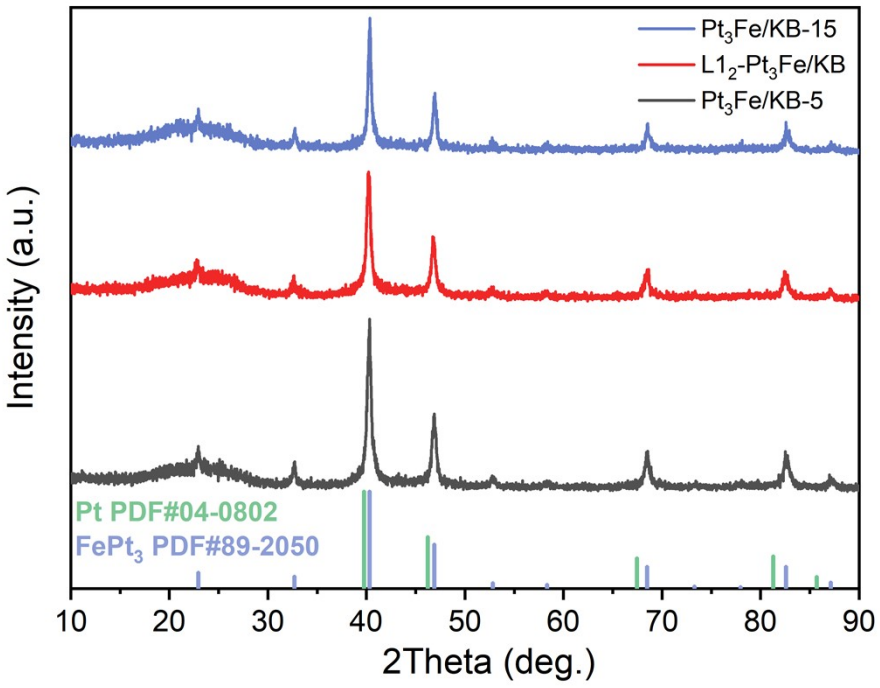

Figure S12. XRD patterns of the Pt_3Fe/KB–5, $L1_2$–Pt_3Fe/KB and Pt_3Fe/KB–15, respectively.

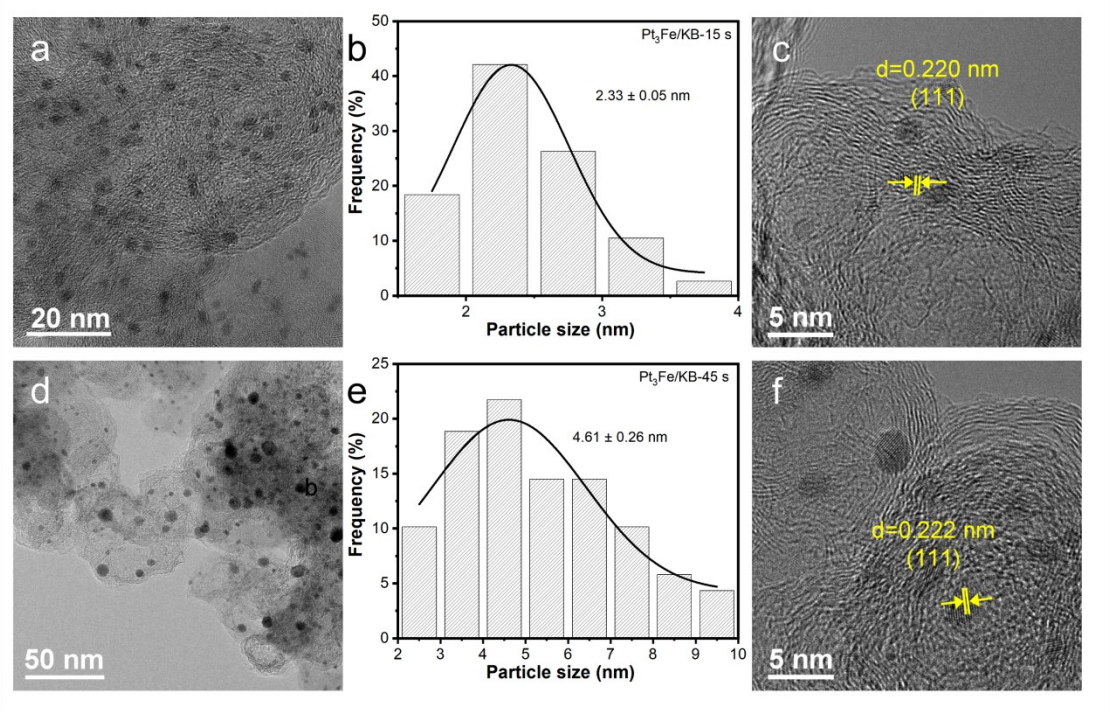

Figure S13. TEM images, the corresponding particle size distributions and HR–TEM images of (a–c) Pt_3Fe/KB–15 s and (d–f) Pt_3Fe/KB–45 s, respectively.

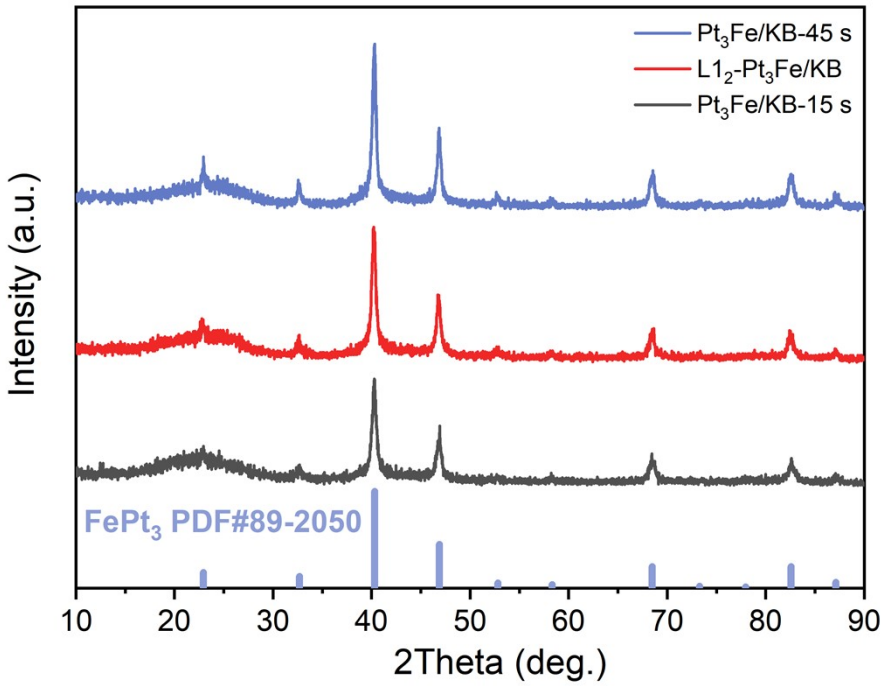

Figure S14. XRD patterns of the Pt_3Fe/KB–15 s, $L1_2$–Pt_3Fe/KB, Pt_3Fe/KB–45 s, respectively.

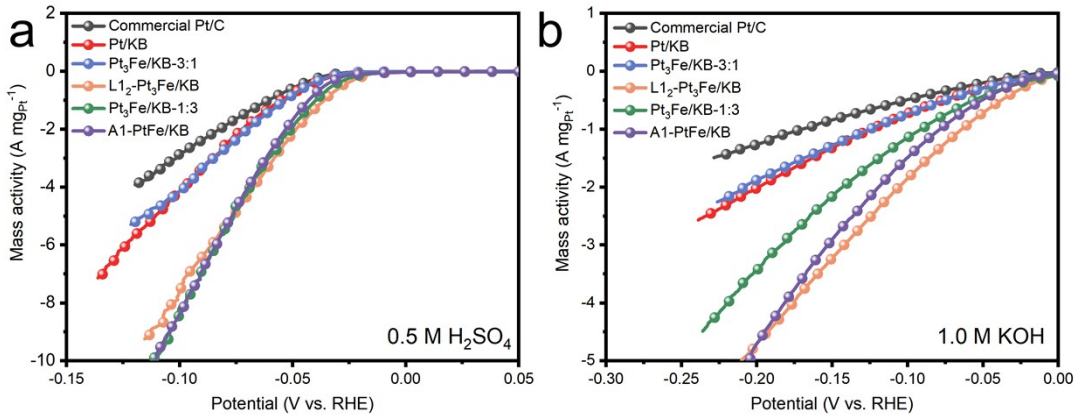

Figure S15. Mass activities curves of Commercial Pt/C, Pt/KB, Pt_3Fe/KB–3:1, $L1_2$–Pt_3Fe/KB, Pt_3Fe/KB–1:3, A1–PtFe/KB catalysts in (a) 0.5 M H_2SO_4 and (b) 1.0 M KOH.

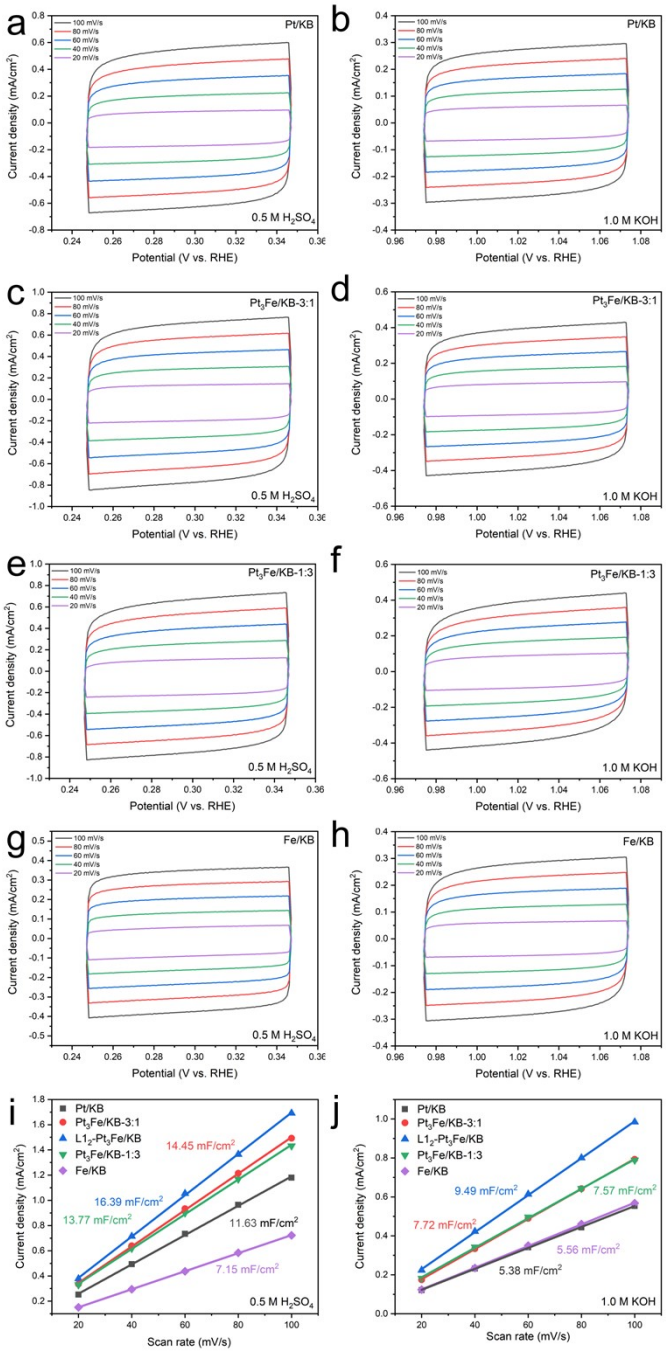

Figure S16. Cyclic voltammetry (20–100 mV/s) of the Pt/KB, Pt_3Fe/KB–3:1, Pt_3Fe/KB–1:3, and Fe/KB catalysts in (a, c, e, g) 0.5 M H_2SO_4 and (b, d, f, h) 1.0 M KOH. C_{dl} fitting results of the Pt/KB, Pt_3Fe/KB–3:1, Pt_3Fe/KB–1:3, and Fe/KB catalysts in (i) 0.5 M H_2SO_4 and (j) 1.0 M KOH.

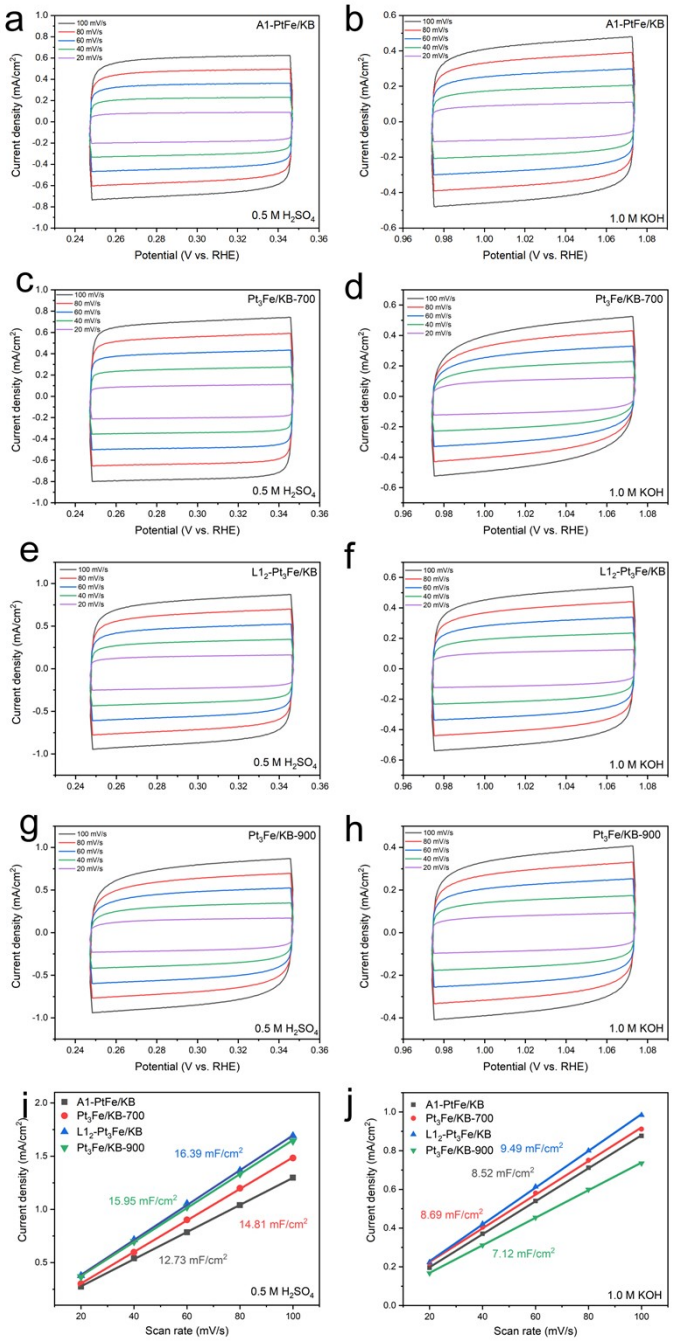

Figure S17. Cyclic voltammetry (20–100 mV/s) of the A1–PtFe/KB, Pt_3Fe/KB–700, $L1_2$–Pt_3Fe/KB, and Pt_3Fe/KB–900 catalysts in (a, c, e, g) 0.5 M H_2SO_4 and (b, d, f, h) 1.0 M KOH. C_{dl} fitting results of the A1–PtFe/KB, Pt_3Fe/KB–700, $L1_2$–Pt_3Fe/KB, and Pt_3Fe/KB–900 catalysts in (i) 0.5 M H_2SO_4 and (j) 1.0 M KOH.

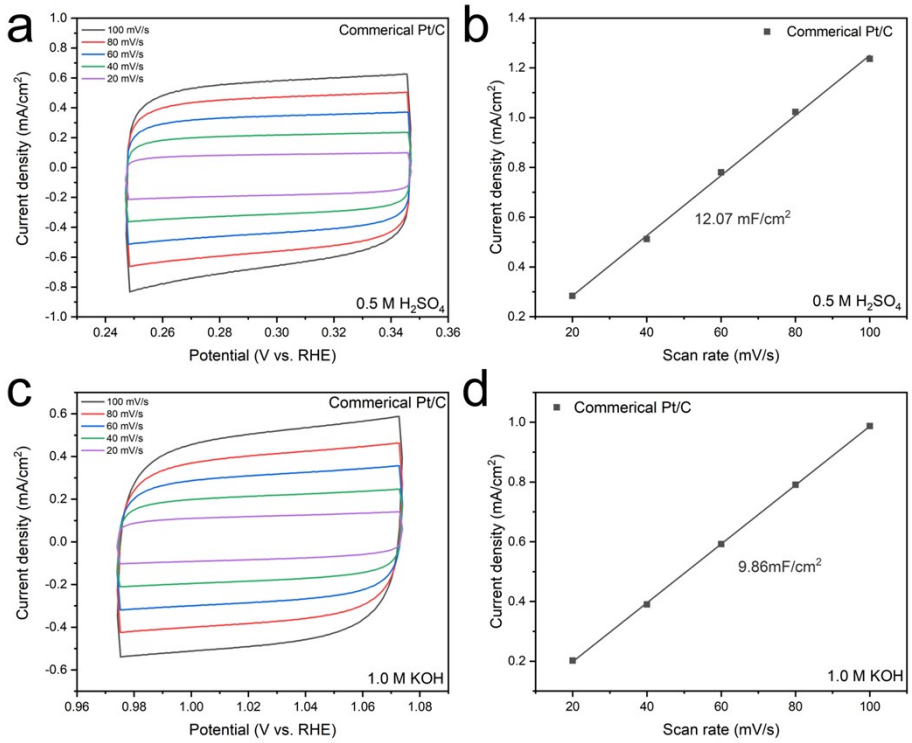

Figure S18. Cyclic voltammetry (20–100 mV/s) of the Commercial Pt/C in (a) 0.5 M H_2SO_4 and (c) 1.0 M KOH. C_{dl} fitting results of the Commercial Pt/C in (b) 0.5 M H_2SO_4 and (d) 1.0 M KOH.

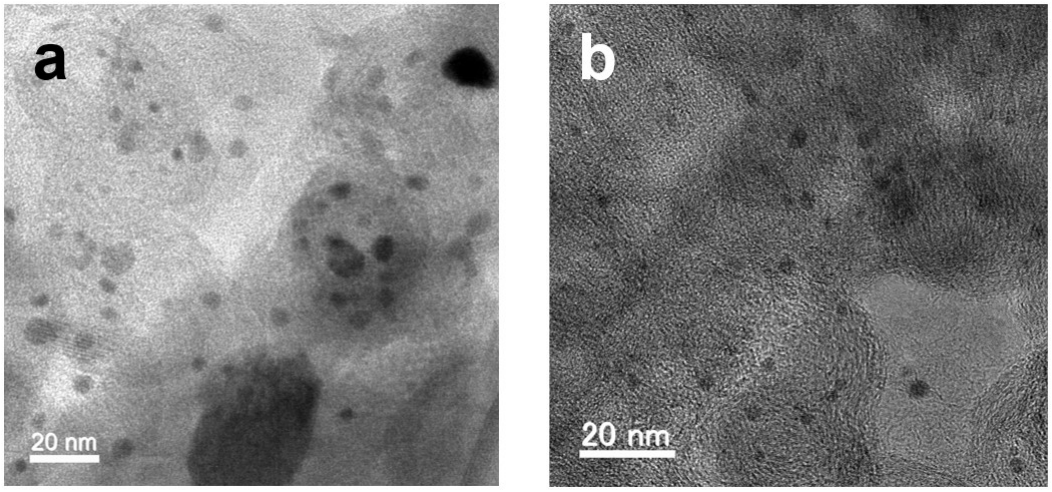

Figure S19. TEM images of the (a) Commercial Pt/C and (b) $L1_2$–Pt_3Fe/KB after 20 h stability test in 1.0 M KOH.

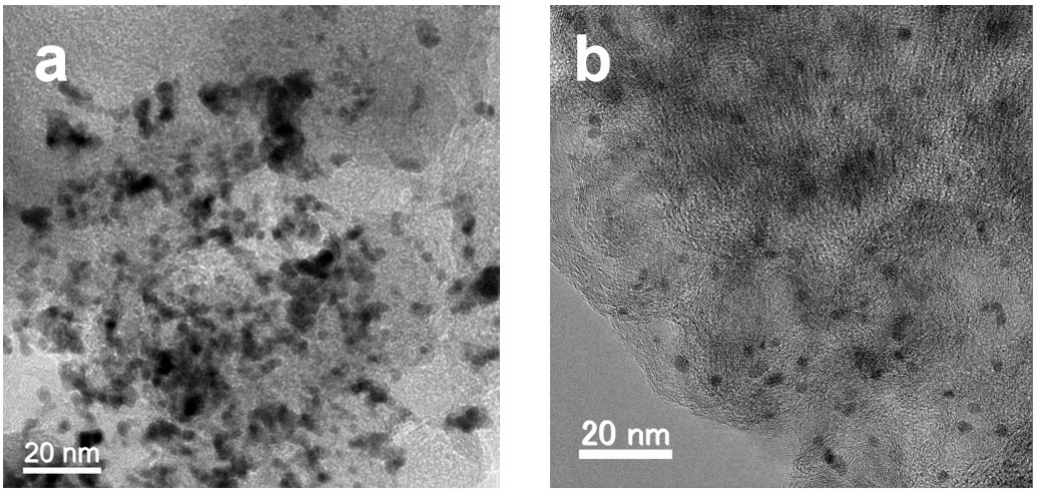

Figure S20. TEM images of the (a) Commercial Pt/C and (b) $L1_2$–Pt_3Fe/KB after 20 h stability test in 0.5 M H_2SO_4.

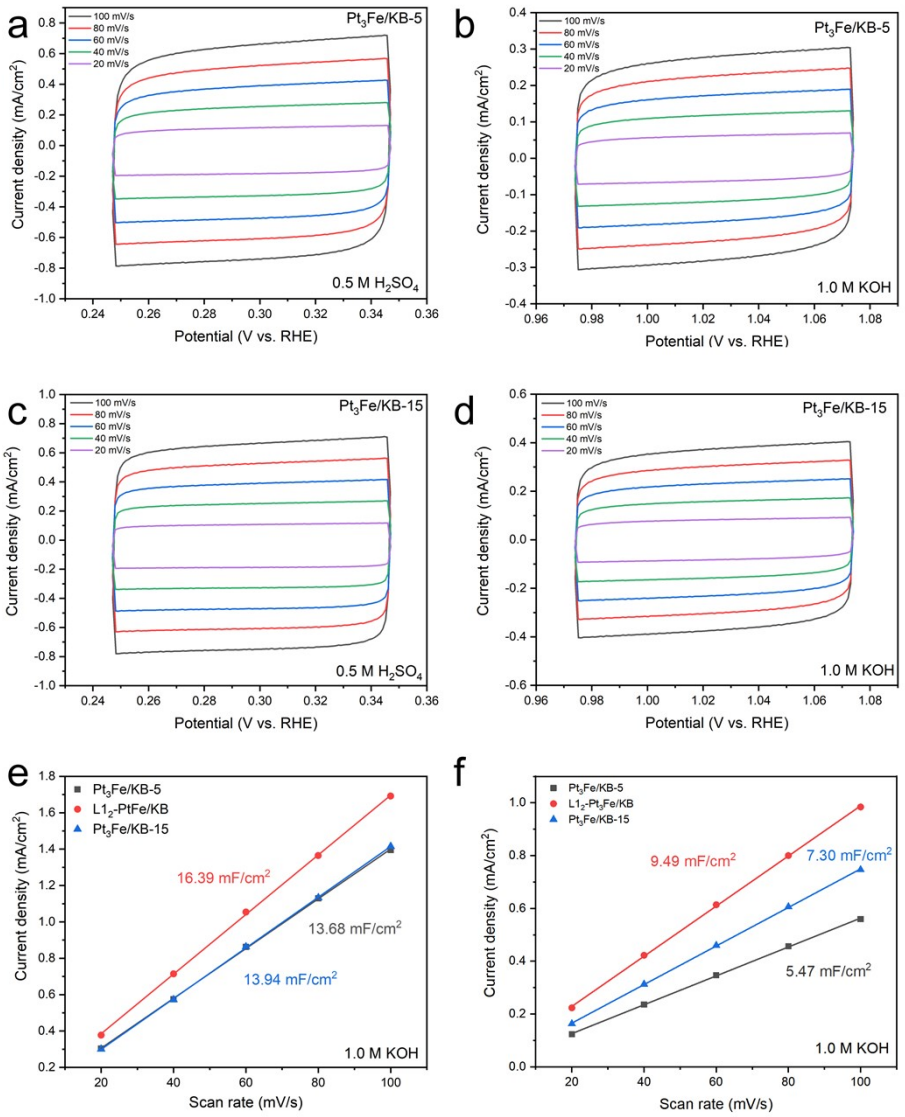

Figure S21. Cyclic voltammetry (20–100 mV/s) of the Pt_3Fe/KB–5, $L1_2$–Pt_3Fe/KB, Pt_3Fe/KB–15 catalysts in (a, c) 0.5 M H_2SO_4 and (b, d) 1.0 M KOH. C_{dl} fitting results of the Pt_3Fe/KB–5, $L1_2$–Pt_3Fe/KB, Pt_3Fe/KB–15 catalysts in (e) 0.5 M H_2SO_4 and (f) 1.0 M KOH.

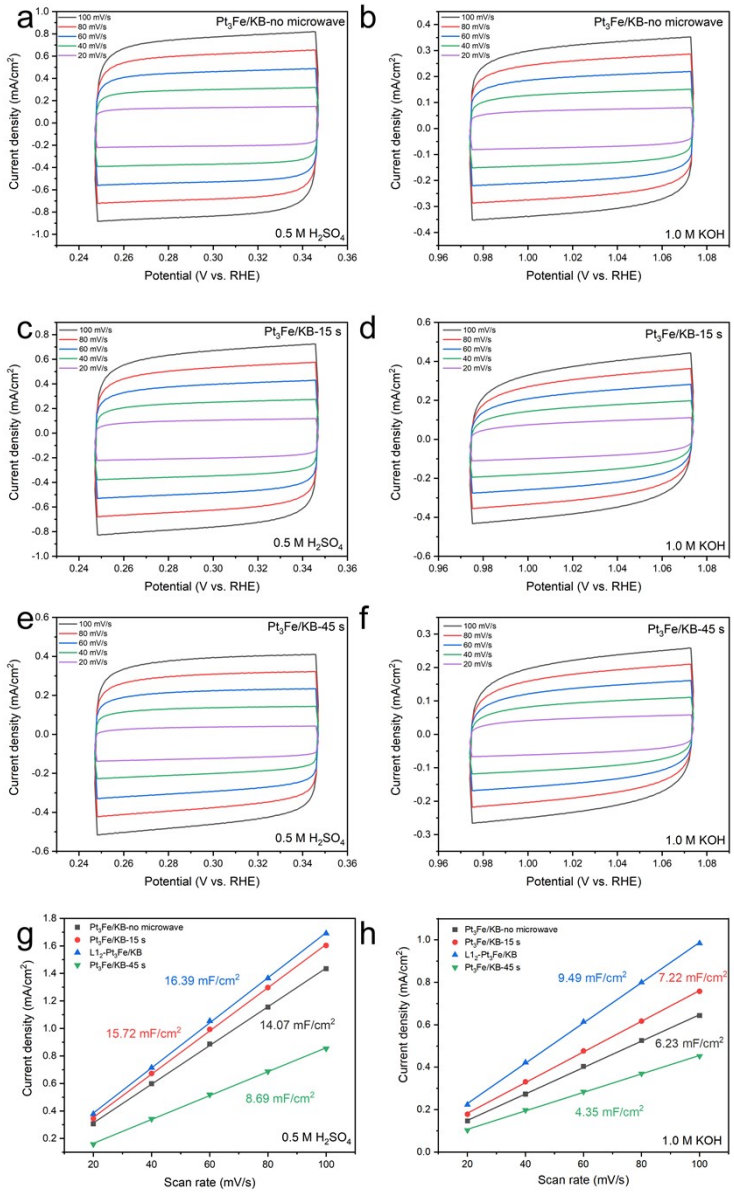

Figure S22. Cyclic voltammetry (20–100 mV/s) of the Pt_3Fe/KB–no microwave, Pt_3Fe/KB–15 s, Pt_3Fe/KB–45 s catalysts in (a, c, e) 0.5 M H_2SO_4 and (b, d, f) 1.0 M KOH. C_{dl} fitting results of the Pt_3Fe/KB–no microwave, Pt_3Fe/KB–15 s, Pt_3Fe/KB–45 s catalysts in (g) 0.5 M H_2SO_4 and (h) 1.0 M KOH.

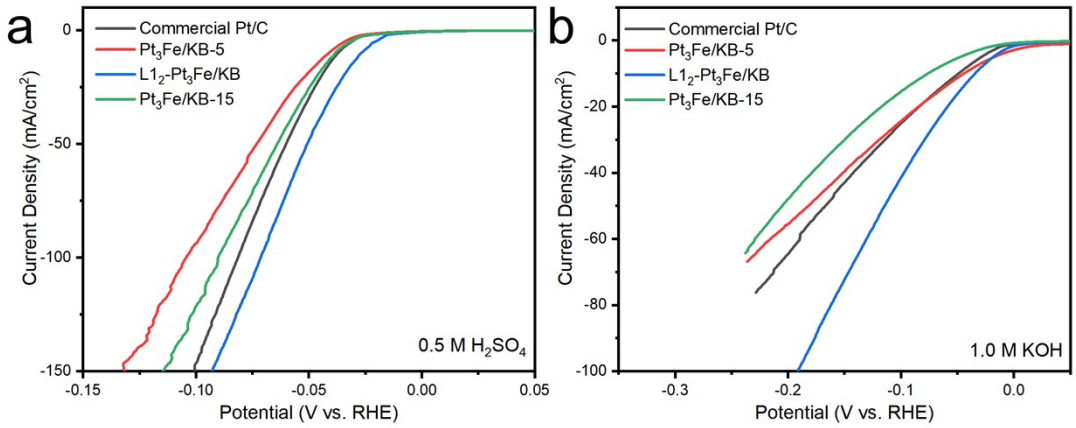

Figure S23. LSV polarization curves of the Pt_3Fe/KB–5, $L1_2$–Pt_3Fe/KB, Pt_3Fe/KB–15 catalysts in (a) 0.5 M H_2SO_4 and (b) 1.0 M KOH.

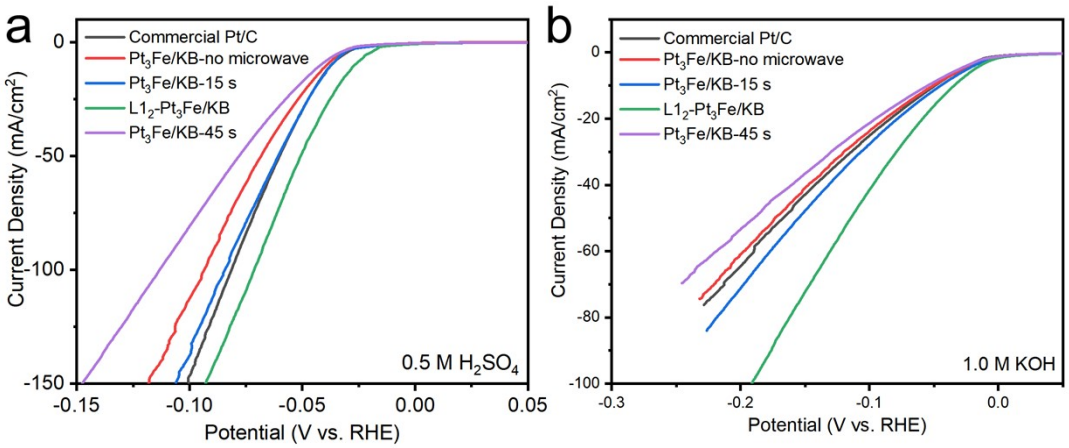

Figure S24. LSV polarization curves of the Pt_3Fe/KB–no microwave, Pt_3Fe/KB–15 s, $L1_2$–Pt_3Fe/KB, Pt_3Fe/KB–45 s catalysts in (a) 0.5 M H_2SO_4 and (b) 1.0 M KOH.

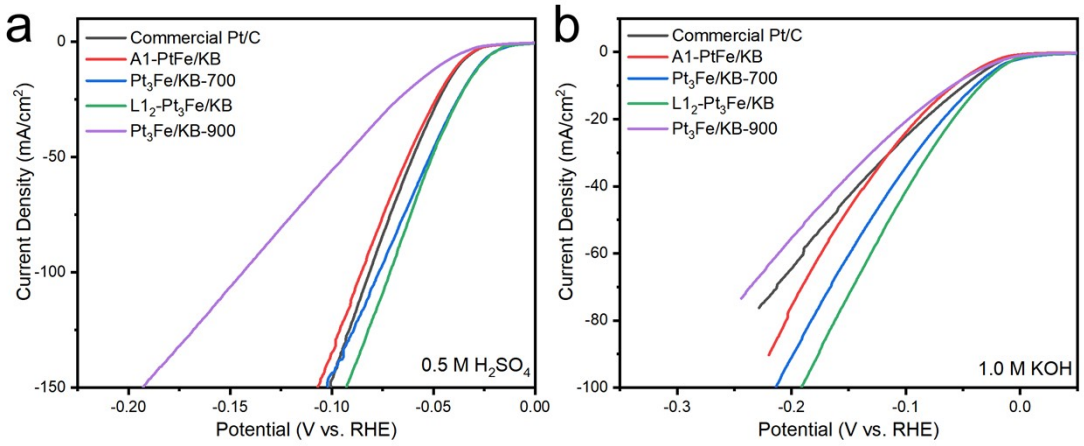

Figure S25. LSV polarization curves of the A1–PtFe/KB, Pt_3Fe/KB–700, $L1_2$–Pt_3Fe/KB, Pt_3Fe/KB–900 catalysts in (a) 0.5 M H_2SO_4 and (b) 1.0 M KOH.

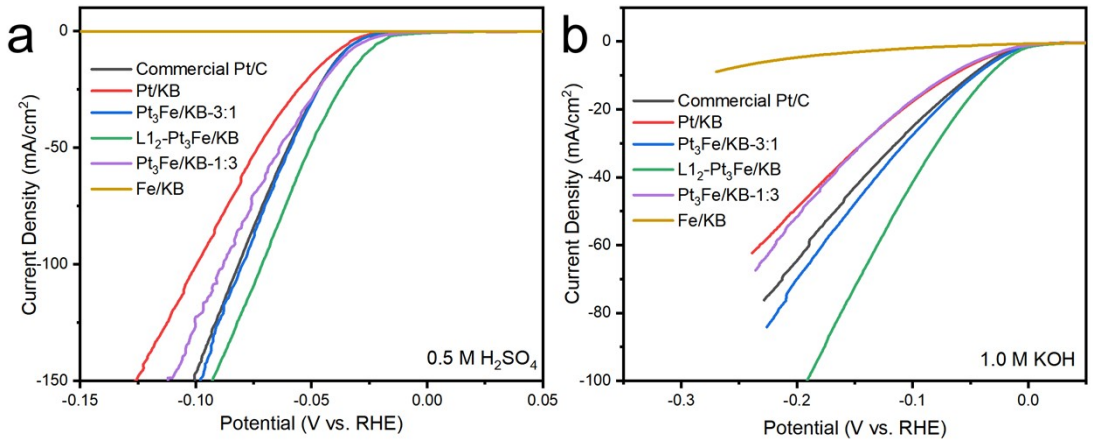

Figure S26. LSV polarization curves of the Pt/KB, Pt_3Fe/KB–3:1, $L1_2$–Pt_3Fe/KB, Pt_3Fe/KB–1:3 and Fe/KB catalysts in (a) 0.5 M H_2SO_4 and (b) 1.0 M KOH.

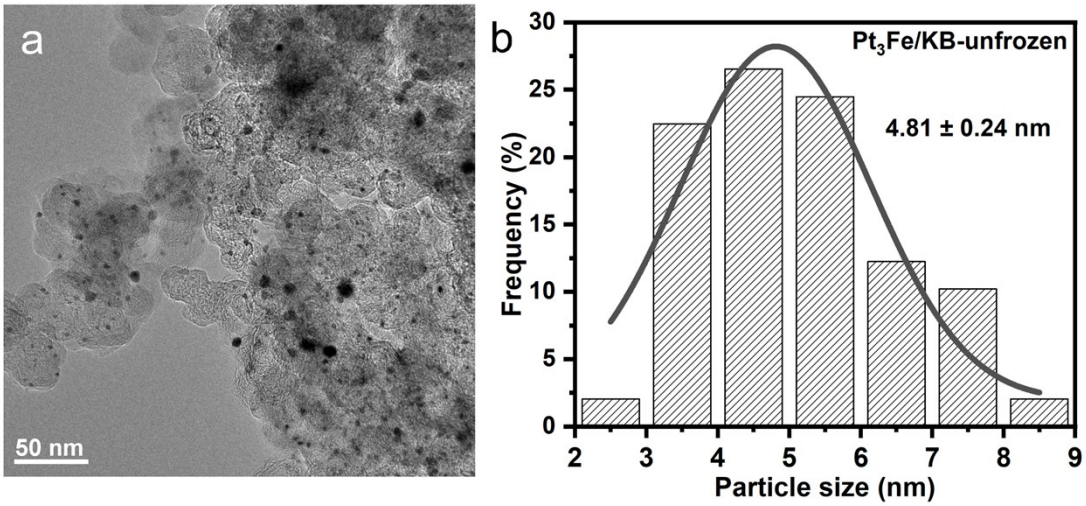

Figure S27. (a) TEM image and (b) the corresponding particle size distribution of Pt_3Fe/KB–unfrozen.

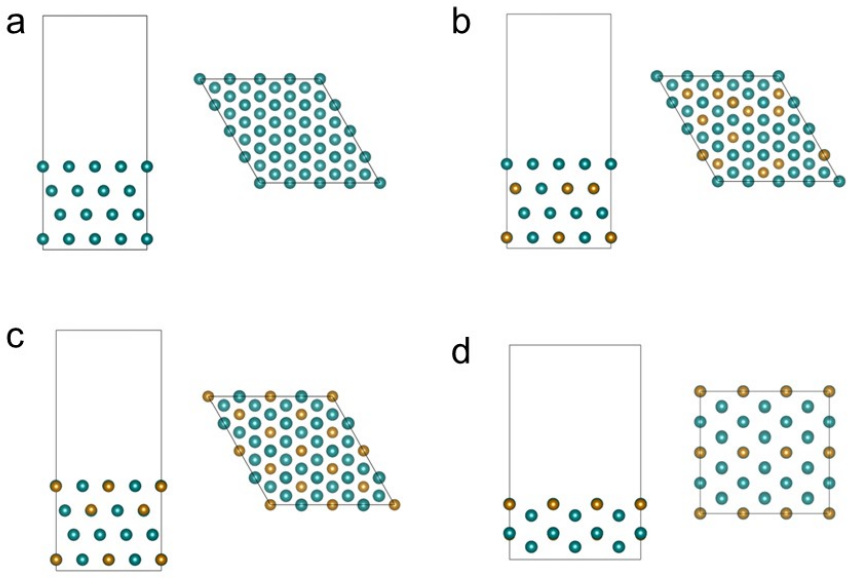

Figure S28. The established atomic models of (a) Pt (111), (b) A1–PtFe (111), (c) $L1_2$–Pt_3Fe (111) and (d) $L1_2$–Pt_3Fe (110) for DFT calculations. The Pt and Fe atoms were shown in green and yellow. (Side view on the left, top view on the right.)

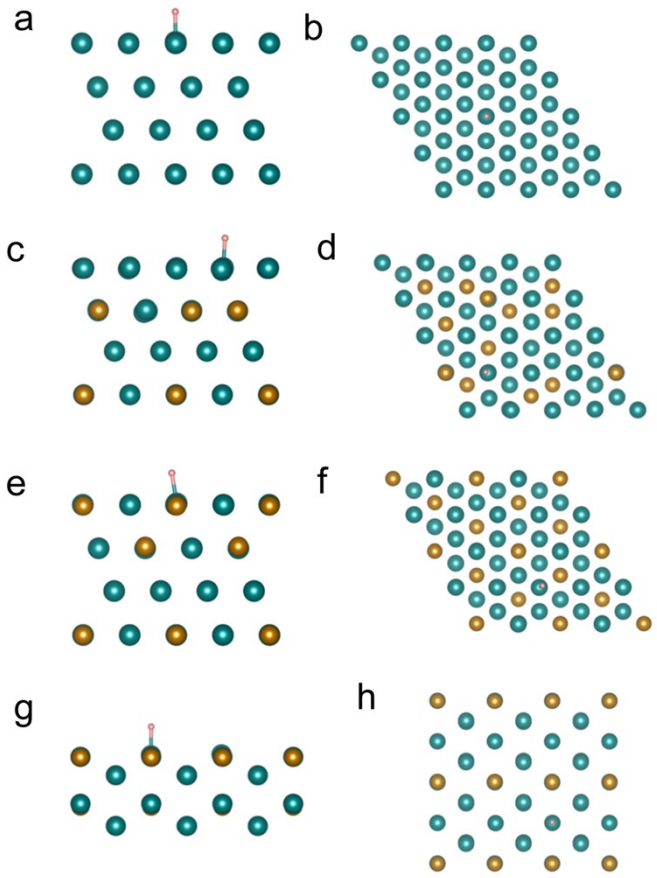

Figure S29. Chemisorption atomic models with H^* intermediates on the surfaces of (a, b) Pt (111), (c, d) A1–PtFe (111), (e, f) $L1_2$–Pt_3Fe (111), (g, h) $L1_2$–Pt_3Fe (110) (side and top views for each pair, respectively.)

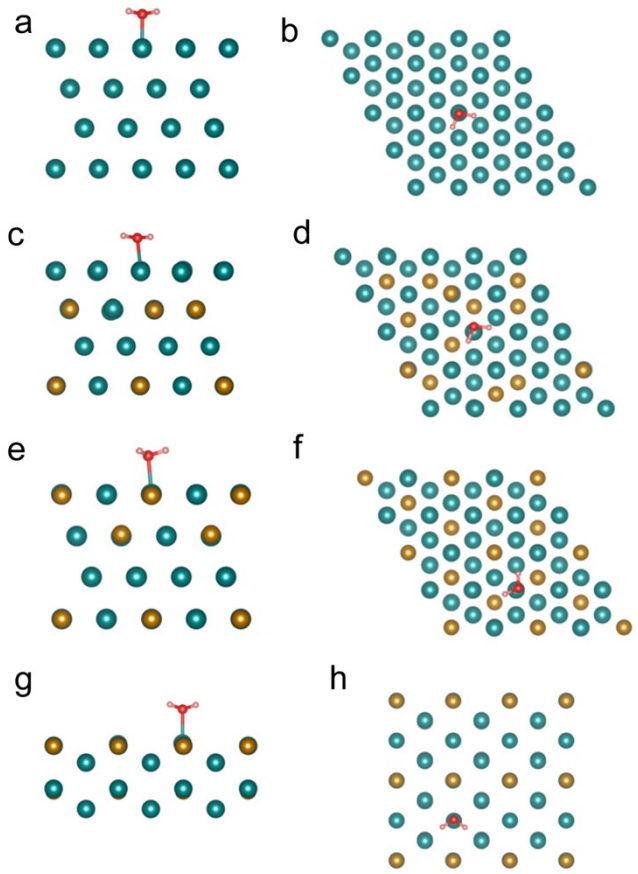

Figure S30. Chemisorption atomic models with H_2O^* on the surfaces of (a, b) Pt(111), (c, d) A1–PtFe(111), (e, f) $L1_2$–Pt_3Fe(111), and (g, h) $L1_2$–Pt_3Fe(110) (side and top views for each pair, respectively).

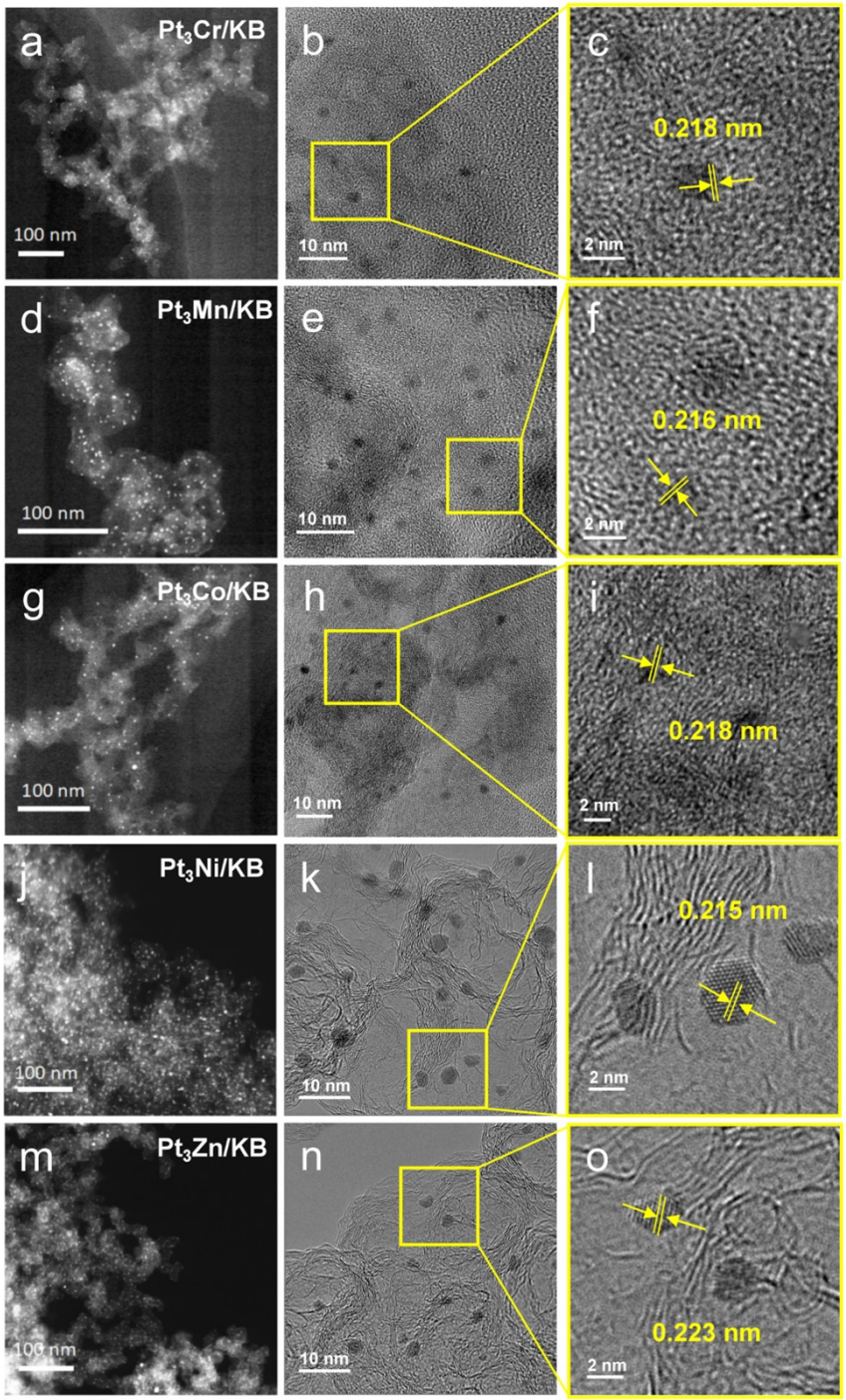

Figure S31. HAADF–STEM images, TEM images, and HR–TEM images of (a–c) Pt_3Cr/KB, (d–f) Pt_3Mn/KB, (g–i) Pt_3Co/KB, (j–l) Pt_3Ni/KB, and (m–o) Pt_3Zn/KB, respectively. (c, f, i, l, and o are enlarged views of the boxed areas in b, e, h, k, and n, respectively.)

Table S1. The Pt and Fe content in the samples tested by ICP–OES.

Sample	Pt wt%	Fe wt%
Pt/KB	9.51	–
A1–PtFe/KB	6.30	0.66
$L1_2$–Pt_3Fe/KB	8.78	1.72
Pt_3Fe/KB–1:3	5.89	1.62
Pt_3Fe/KB–3:1	14.6	1.39

Table S2. The fitting results of Pt L_3–edeg EXAFS spectra for A1–PtFe/KB, $L1_2$–Pt_3Fe/KB, Pt foil and Pt_2O.

Sample	Path	CN	R(Å)	σ^2(Å^2)	R facter
A1–PtFe/KB	Pt–O	0.7 ± 0.2	2.015-0.04 ± 0.03	0.003	0.022
	Pt–Fe	1.4 ± 0.7	2.751-0.056 ± 0.01	0.01	
	Pt–Pt	5.2 ± 1.6	2.751-0.026 ± 0.012	0.005 ± 0.002	
$L1_2$–Pt_3Fe/KB	Pt–O	0.4 ± 0.2	2.015-0.01 ± 0.04	0.003	0.009
	Pt–Fe	2.8 ± 0.9	2.751-0.053 ± 0.019	0.01 ± 0.004	
	Pt–Pt	4.7 ± 0.5	2.751-0.032 ± 0.007	0.003	

Table S3. Summarized alkaline HER performance of some reported atomic level catalysis with present work.

Electrocatalysts	Overpotential (mV) (10 mA cm^{-2})	Tafel slope (mV dec^{-1})	Ref.
$L1_2$–Pt_3Fe/KB	35	39	This work
CoNi–inf	72	57	[7]
Pt_1Ru_x@C	48.7	55.6	[8]
Pt/np–$Co_{0.85}Se$	58	155	[9]
Pt_1–Mo_2C–C	155	64	[10]
$Pd_{(100)}$–Pt	71	31	[11]
ß–$Ni(OH)_2$/Pt	108	39	[12]
hcp–PtNi	65	78	[13]
Pt	58	30	[14]
SA–Pt/MoS_2	123	77	[15]
CoPx@CNS	91	129	[16]
RuNi–alloy@SC	93	96	[17]
Pt/GO	144	75.9	[18]
Fe–Ni_3S_2	102	101	[19]
$NiWO_4$/Ni_3S_2	136	122	[20]
$NiCo_2S_4$/ReS_2	85	78.3	[21]
Ce–CoP@CC	81	68.7	[22]
NiCo–SAD–NC	61	55	[23]
Pt/MOF–O	66	101.6	[24]
IrCo@NC	82	56	[25]
Pt NPs@CF	49	36	[26]
Ru SAs–NiP	57	75	[27]

Table S4. Comparison with recently reported OWS performance in 1.0 M KOH.

Catalyst	Cell voltage (V)	Ref.
RuNiFe@NF	1.60	[28]
Ru–G/CC@RuH_2O/CC	1.67	[29]
CoRu–MoS_2	1.67	[30]
Ru/RuO_2/NC || RuO_2	1.58	[31]
Ru–FeRu@C/NC || Ru–Fe Ru@C/NC	1.63	[31]
PdP_2@CB	1.72	[32]
IrCo@NC/GCE	1.62	[25]
Ir/Ni_3Fe/rGO	1.58	[33]
Co_3Mo_3N/Co_4N/Co	1.580	[34]
$L1_2$–Pt_3Fe/KB || IrO_2	1.59	This work

Table S5. Summarized acidic HER performance of some reported atomic level catalysis with present work.

Electrocatalysts	Overpotential (mV) (10 mA cm^{-2})	Tafel slope ($mV\ dec^{-1}$)	Ref.
$L1_2$–Pt_3Fe/KB	27	19	This work
$Pt_{61}La_{39}$@KB	38	29	[35]
Pt SAs/MoS_2	44	34.8	[15]
PtCo CNFs	63	28	[36]
CPt @ZIF–67	50	27.1	[37]
PtRu/RFCs	46.6	46.7	[38]
Pt–MoS_2	67.4	76.2	[39]
PtRu@C_2–N	52	31	[40]
Pt_3Co@NCNT	42	27.2	[41]
PtCo@NCNT	64	48.5	[41]
Pt/np–$Co_{0.85}Se$	58	26	[9]
PtML/Ag NF/Ni foam	70	53	[42]
Pt@PCM	105	63.7	[43]
NiCo–SAD–NC	55	31.5	[23]
PtCu/WO_3@CF	41	45.9	[44]
Pt_1/NMHCS	40	56	[45]
PtN_x/TiO_2	67	34	[46]
Br–Ru/RuP_2	56	36	[47]
N–RuS_2/Ru	76	53	[48]
$RuVO_2$	46	39.1	[49]
IrO_2–RuO_2/KB	82	37	[50]

Table S6. Comparison with recently reported OWS performance in 0.5 M H_2SO_4.

Catalyst	Cell voltage (V)	Ref.
RuO_2–WC NPs	1.66	[51]
CoP–InNC@CNT || CoP–InNC@CNT	1.58	[52]
IrNi NFs CFP || IrNi NFs CFP	1.6	[53]
RuSAs@$MoSe_2$–MXene || RuO_2	1.626	[54]
Pt/C/CP || RuO_2/CP	1.66	[51]
Mo–Co_9S_8@C || Mo–Co_9S_8@C	1.68	[55]
Co–MoS_2	1.90	[56]
Mn–Doped FeP/$Co_3(PO_4)_2$ || Mn–Doped FeP/$Co_3(PO_4)_2$	1.75	[57]
p–FGDY/CC || p–FGDY/CC	1.8	[58]
$L1_2$–Pt_3Fe/KB || IrO_2	1.58	This work

Table S7. Comparison of the ordering degree of $L1_2$–Pt_3Fe/KB, A1–PtFe/KB with previously reported Pt–based intermetallic catalysts.

Sample	Ordering degree (%)	Ref.
A1–PtFe/KB	0	This work
$L1_2$–Pt_3Fe/KB	79.0	This work
Pt_3Fe/KB–700	57.0	This work
Pt_3Fe/KB–900	81.0	This work
Pt_3Fe/KB–3:1	38.7	This work
Pt_3Cr/KB	43.17	This work
Pt_3Mn/KB	79.59	This work
Pt_3Co/KB	44.85	This work
Pt_3Zn/KB	30.72	This work
Pt_3Al	9.5[b]	59
Pt_3Ti	37.9[c]	60
Pt_3Ti	34.1[c]	61
Pt_3V	48.9[c]	60
Pt_3V	35.9[b]	2
Pt_3Cr	52.2[c]	62
Pt_3Cr	51.7[c]	63
Pt_3Mn	25.3[c]	63
Pt_3Mn	23.2[c]	64
Pt_3Mn	41.2[b]	65
Pt_3Fe	28.0[c]	63
Pt_3Fe	37.3[b]	65
Pt_3Fe	68.2[c]	66
Pt_3Fe	79.7[c]	2
Pt_3Co	34.2[c]	63
Pt_3Co	23.4[c]	67
Pt_3Co	34.8[c]	68
Pt_3Co	29.1[b]	69
Pt_3Zn	43.8[d]	2
Pt_3Zn	47.1[c]	70
$L1_0$–$Pt_{50}Fe_{45}Sn_5$	74[d]	4

b S(100)/[S(111)+S(200)]

c S(110)/S(111)

d S(110)/[S(111)+S(200)+S(002)] or S(110)/[S(111)+S(200)]

Table S8. Comparison of the particle size of $L1_2$–Pt_3Fe/KB with recently reported ordered Pt–based nanoparticles.

Sample	Particle size (nm)	Ref.
$L1_2$–Pt_3Fe/KB	2.84 ± 0.05	This work
Pt_3Cr/KB	2.81 ± 0.06	This work
Pt_3Mn/KB	2.95 ± 0.06	This work
Pt_3Co/KB	2.21 ± 0.04	This work
Pt_3Zn/KB	2.15 ± 0.03	This work
Ordered Pt_1Bi_2	13.2	71
Ordered PtCo	8.9	72
Ordered PtFe	8.8 ± 0.5	73
Pt_3Co–700/C	7.2	67
Ordered Pt_3Ti/C	6.1 ± 0.5	60
Ordered Pt_3V/C	5.8 ± 0.6	60
Ordered PtCu/C–700	6.0	74
Ordered PtCo	5.3	75
$L1_0$–PtMn	4.6	3
$L1_2$–Pt_3Mn	4.5	3
$L1_0$–$Pt_{50}Fe_{45}Sn_5$	4.5	4
O–Pt_3Fe/rGO	3.7	76
PNAC–o–Pt_3Fe/C	4.0	77
PtNi	5.0	78
PtCo	4.6	78
PtFe	3.5	78
$L1_0$–PtCo/Co–N–PCNF NPs	7.4	79
$L1_0$–PtCoM’	5.0	80
Pt_3Fe/NMCS–A	2	81
Pt_3Zn	2.12	2
Pt_3Fe	3.59	2

References

1 B. Ravel and M. Newville, *J. Synchrotron Radiat.*, 2005, **12**, 537–541.

2 C.-L. Yang, L.-N. Wang, P. Yin, J. Liu, M.-X. Chen, Q.-Q. Yan, Z.-S. Wang, S.-L. Xu, S.-Q. Chu, C. Cui, H. Ju, J. Zhu, Y. Lin, J. Shui and H.-W. Liang, *Science*, 2021, **374**, 459–464.

3 W. Yan, X. Wang, M. Liu, K. Ma, L. Wang, Q. Liu, C. Wang, X. Jiang, H. Li, Y. Tang and G. Fu, *Adv. Funct. Mater.*, 2024, **34**, 2310487.

4 J. Liang, Y. Wan, H. Lv, X. Liu, F. Lv, S. Li, J. Xu, Z. Deng, J. Liu, S. Zhang, Y. Sun, M. Luo, G. Lu, J. Han, G. Wang, Y. Huang, S. Guo and Q. Li, *Nat. Mater.*, 2024, **23**, 1259–1267.

5 G. Kresse and D. Joubert, *Phys. Rev. B*, 1999, **59**, 1758–1775.

6 J. P. Perdew, K. Burke and M. Ernzerhof, *Phys. Rev. Lett.*, 1996, **77**, 3865–3868.

7 X. Tan, S. Geng, Y. Ji, Q. Shao, T. Zhu, P. Wang, Y. Li and X. Huang, *Adv. Mater.*, 2020, **32**, 2002857.

8 X. Zhu, M. Fang, B. Yang, M. Zhan, S. Ke, F. Yang, X. Wu, Y. Liu, Z. Huang and X. Min, *J. Mater. Chem. A*, 2024, **12**, 4108–4122.

9 K. Jiang, B. Liu, M. Luo, S. Ning, M. Peng, Y. Zhao, Y.-R. Lu, T.-S. Chan, F. M. F. De Groot and Y. Tan, *Nat. Commun.*, 2019, **10**, 1743.

10 S. Niu, J. Yang, H. Qi, Y. Su, Z. Wang, J. Qiu, A. Wang and T. Zhang, *J. Energy Chem.*, 2021, **57**, 371–377.

11 J. Fan, K. Qi, L. Zhang, H. Zhang, S. Yu and X. Cui, *ACS Appl. Mater. Interfaces*, 2017, **9**, 18008–18014.

12 X. Yu, J. Zhao, L.-R. Zheng, Y. Tong, M. Zhang, G. Xu, C. Li, J. Ma and G. Shi, *ACS Energy Lett.*, 2018, **3**, 237–244.

13 Z. Cao, Q. Chen, J. Zhang, H. Li, Y. Jiang, S. Shen, G. Fu, B. Lu, Z. Xie and L. Zheng, *Nat. Commun.*, 2017, **8**, 15131.

14 H. Hong, H. Y. Kim, W. I. Cho, H. C. Song, H. C. Ham, K. Chae, F. Marques Mota, J. Y. Kim and D. H. Kim, *J. Mater. Chem. A*, 2023, **11**, 5328–5336.

15 J. Zhu, Y. Tu, L. Cai, H. Ma, Y. Chai, L. Zhang and W. Zhang, *Small*, 2022, **18**, 2104824.

16 C. Hou, L. Zou, Y. Wang and Q. Xu, *Angew. Chem. Int. Ed.*, 2020, **59**, 21360–21366.

17 X. Bai, Q.-Q. Pang, X. Du, S.-S. Yi, S. Zhang, J. Qian, X.-Z. Yue and Z.-Y. Liu, *Chem. Eng. J.*, 2021, **417**, 129319.

18 X. Luo, H. Xiao, J. Li, P. Yuan, B. Du, H. Zheng, D. Li and Y. Chen, *J. Electroanal. Chem.*, 2023, **939**, 117476.

19 D. Li, W. Wan, Z. Wang, H. Wu, S. Wu, T. Jiang, G. Cai, C. Jiang and F. Ren, *Adv. Energy Mater.*, 2022, **12**, 2201913.

20 S. Huang, Y. Meng, Y. Cao, F. Yao, Z. He, X. Wang, H. Pan and M. Wu, *Appl. Catal. B Environ.*, 2020, **274**, 119120.

21 C. Pei, M. Kim, Y. Li, C. Xia, J. Kim, W. So, X. Yu, H. S. Park and J. K. Kim, *Adv. Funct. Mater.*, 2023, **33**, 2210072.

22 M. Li, X. Wang, K. Liu, Z. Zhu, H. Guo, M. Li, H. Du, D. Sun, H. Li, K. Huang, Y. Tang and G. Fu, *Adv. Energy Mater.*, 2023, **13**, 2301162.

23 A. Kumar, V. Q. Bui, J. Lee, L. Wang, A. R. Jadhav, X. Liu, X. Shao, Y. Liu, J. Yu, Y. Hwang, H. T. D. Bui, S. Ajmal, M. G. Kim, S.-G. Kim, G.-S. Park, Y. Kawazoe and H. Lee, *Nat. Commun.*, 2021, **12**, 6766.

24 M. Wang, Y. Xu, C.-K. Peng, S.-Y. Chen, Y.-G. Lin, Z. Hu, L. Sun, S. Ding, C.-W. Pao, Q. Shao and X. Huang, *J. Am. Chem. Soc.*, 2021, **143**, 16512–16518.

25 Y. Zhou, L. Zhang, H. Suo, W. Hua, S. Indris, Y. Lei, W. Lai, Y. Wang, Z. Hu, H. Liu, S. Chou and S. Dou, *Adv. Funct. Mater.*, 2021, **31**, 2101797.

26 Q. Li, Z. Deng, D. Tao, J. Pan, W. Xu, Z. Zhang, H. Zhong, Y. Gao, Q. Shang, Y. Ni, X. Li, Y. Chen and Q. Zhang, *Adv. Funct. Mater.*, 2024, **34**, 2411283.

27 K. Wu, K. Sun, S. Liu, W.-C. Cheong, Z. Chen, C. Zhang, Y. Pan, Y. Cheng, Z. Zhuang, X. Wei, Y. Wang, L. Zheng, Q. Zhang, D. Wang, Q. Peng, C. Chen and Y. Li, *Nano Energy*, 2021, **80**, 105467.

28 M. Zhao, H. Li, W. Li, J. Li, L. Yi, W. Hu and C. M. Li, *Chem. – Eur. J.*, 2020, **26**, 17091–17096.

29 M. You, X. Du, X. Hou, Z. Wang, Y. Zhou, H. Ji, L. Zhang, Z. Zhang, S. Yi and D. Chen, *Appl. Catal. B Environ.*, 2022, **317**, 121729.

30 I. S. Kwon, T. T. Debela, I. H. Kwak, Y. C. Park, J. Seo, J. Y. Shim, S. J. Yoo, J. Kim, J. Park and H. S. Kang, *Small*, 2020, **16**, 2000081.

31 W. Feng, Y. Feng, J. Chen, H. Wang, Y. Hu, T. Luo, C. Yuan, L. Cao, L. Feng and J. Huang, *Chem. Eng. J.*, 2022, **437**, 135456.

32 F. Luo, Q. Zhang, X. Yu, S. Xiao, Y. Ling, H. Hu, L. Guo, Z. Yang, L. Huang, W. Cai and H. Cheng, *Angew. Chem. Int. Ed.*, 2018, **57**, 14862–14867.

33 Y. Li, Y.-C. Miao, C. Yang, Y.-X. Chang, Y. Su, H. Yan and S. Xu, *Chem. Eng. J.*, 2023, **451**, 138548.

34 Y. Liu, L. Wang, R. Hübner, J. Kresse, X. Zhang, M. Deconinick, Y. Vaynzof, I. M. Weidinger and A. Eychmüller, *Angew. Chem. Int. Ed.*, 2024, **63**, e202319239.

35 N. Nie, D. Zhang, Z. Wang, Y. Qin, X. Zhai, B. Yang, J. Lai and L. Wang, *Small*, 2021, **17**, 2102879.

36 T. Yang, H. Zhu, M. Wan, L. Dong, M. Zhang and M. Du, *Chem. Commun.*, 2016, **52**, 990–993.

37 Y. Qin, X. Han, S. Gadipelli, J. Guo, S. Wu, L. Kang, J. Callison and Z. Guo, *J. Mater. Chem. A*, 2019, **7**, 6543–6551.

38 K. Li, Y. Li, Y. Wang, J. Ge, C. Liu and W. Xing, *Energy Environ. Sci.*, 2018, **11**, 1232–1239.

39 A. Shan, X. Teng, Y. Zhang, P. Zhang, Y. Xu, C. Liu, H. Li, H. Ye and R. Wang, *Nano Energy*, 2022, **94**, 106913.

40 C. Li, L. Zhang, Y. Zhang, Y. Zhou, J. Sun, X. Ouyang, X. Wang, J. Zhu and Y. Fu, *Chem. Eng. J.*, 2022, **428**, 131085.

41 S. L. Zhang, X. F. Lu, Z. Wu, D. Luan and X. W. (David) Lou, *Angew. Chem. Int. Ed.*, 2021, **60**, 19068–19073.

42 M. Li, Q. Ma, W. Zi, X. Liu, X. Zhu and S. (Frank) Liu, *Sci. Adv.*, 2015, **1**, e1400268.

43 H. Zhang, P. An, W. Zhou, B. Y. Guan, P. Zhang, J. Dong and X. W. (David) Lou, *Sci. Adv.*, 2018, **4**, eaao6657.

44 L. Liu, Y. Wang, Y. Zhao, Y. Wang, Z. Zhang, T. Wu, W. Qin, S. Liu, B. Jia, H. Wu, D. Zhang, X. Qu, M. Chhowalla and M. Qin, *Adv. Funct. Mater.*, 2022, **32**, 2112207.

45 P. Kuang, Y. Wang, B. Zhu, F. Xia, C. Tung, J. Wu, H. M. Chen and J. Yu, *Adv. Mater.*, 2021, **33**, 2008599.

46 X. Cheng, Y. Lu, L. Zheng, Y. Cui, M. Niibe, T. Tokushima, H. Li, Y. Zhang, G. Chen, S. Sun and J. Zhang, *Nano Energy*, 2020, **73**, 104739.

47 Z. Wu, Q. Li, G. Xu, W. Jin, W. Xiao, Z. Li, T. Ma, S. Feng and L. Wang, *Adv. Mater.*, 2024, **36**, 2311018.

48 Y. Xu, X. Gao, J. Zhang and D. Gao, *RSC Adv.*, 2020, **10**, 17862–17868.

49 Z. Niu, Z. Lu, Z. Qiao, S. Wang, X. Cao, X. Chen, J. Yun, L. Zheng and D. Cao, *Adv. Mater.*, 2024, **36**, 2310690.

50 R. Samanta, P. Panda, R. Mishra and S. Barman, *Energy Fuels*, 2022, **36**, 1015–1026.

51 S. Sun, H. Jiang, Z. Chen, Q. Chen, M. Ma, L. Zhen, B. Song and C. Xu, *Angew. Chem. Int. Ed.*, 2022, **61**, e202202519.

52 L. Chai, Z. Hu, X. Wang, Y. Xu, L. Zhang, T. Li, Y. Hu, J. Qian and S. Huang, *Adv. Sci.*, 2020, **7**, 1903195.

53 F. Lv, W. Zhang, W. Yang, J. Feng, K. Wang, J. Zhou, P. Zhou and S. Guo, *Small Methods*, 2020, **4**, 1900129.

54 T. Ma, P. Wang, H.-J. Niu, Z. Che, G. Li and W. Zhou, *Carbon*, 2024, **218**, 118758.

55 S. E. Jun, Y.-H. Kim, J. Kim, W. S. Cheon, S. Choi, J. Yang, H. Park, H. Lee, S.

H. Park, K. C. Kwon, J. Moon, S.-H. Kim and H. W. Jang, *Nat. Commun.*, 2023, **14**, 609.

56 Q. Xiong, X. Zhang, H. Wang, G. Liu, G. Wang, H. Zhang and H. Zhao, *Chem. Commun.*, 2018, **54**, 3859–3862.

57 H. Liu, X. Peng, X. Liu, G. Qi and J. Luo, *ChemSusChem*, 2019, **12**, 1334–1341.

58 C. Xing, Y. Xue, B. Huang, H. Yu, L. Hui, Y. Fang, Y. Liu, Y. Zhao, Z. Li and Y. Li, *Angew. Chem. Int. Ed.*, 2019, **58**, 13897–13903.

59 X. Lang, G. Han, B. Xiao, L. Gu, Z. Yang, Z. Wen, Y. Zhu, M. Zhao, J. Li and Q. Jiang, *Adv. Funct. Mater.*, 2015, **25**, 230–237.

60 Z. Cui, H. Chen, M. Zhao, D. Marshall, Y. Yu, H. Abruña and F. J. DiSalvo, *J. Am. Chem. Soc.*, 2014, **136**, 10206–10209.

61 H. Abe, F. Matsumoto, L. R. Alden, S. C. Warren, H. D. Abruña and F. J. DiSalvo, *J. Am. Chem. Soc.*, 2008, **130**, 5452–5458.

62 Z. Cui, H. Chen, W. Zhou, M. Zhao and F. J. DiSalvo, *Chem. Mater.*, 2015, **27**, 7538–7545.

63 B. Zhang, G. Fu, Y. Li, L. Liang, N. S. Grundish, Y. Tang, J. B. Goodenough and Z. Cui, *Angew. Chem. Int. Ed.*, 2020, **59**, 7857–7863.

64 Y. Kang and C. B. Murray, *J. Am. Chem. Soc.*, 2010, **132**, 7568–7569.

65 H. Chen, D. Wang, Y. Yu, K. A. Newton, D. A. Muller, H. Abruña and F. J. DiSalvo, *J. Am. Chem. Soc.*, 2012, **134**, 18453–18459.

66 C. Jung, C. Lee, K. Bang, J. Lim, H. Lee, H. J. Ryu, E. Cho and H. M. Lee, *ACS Appl. Mater. Interfaces*, 2017, **9**, 31806–31815.

67 D. Wang, H. L. Xin, R. Hovden, H. Wang, Y. Yu, D. A. Muller, F. J. DiSalvo and H. D. Abruña, *Nat. Mater.*, 2013, **12**, 81–87.

68 Y. Xiong, L. Xiao, Y. Yang, F. J. DiSalvo and H. D. Abruña, *Chem. Mater.*, 2018, **30**, 1532–1539.

69 Y. Xiong, Y. Yang, H. Joress, E. Padgett, U. Gupta, V. Yarlagadda, D. N. Agyeman-Budu, X. Huang, T. E. Moylan, R. Zeng, A. Kongkanand, F. A. Escobedo, J. D. Brock, F. J. DiSalvo, D. A. Muller and H. D. Abruña, *Proc. Natl. Acad. Sci.*, 2019, **116**, 1974–1983.

70 J. Zhu, X. Zheng, J. Wang, Z. Wu, L. Han, R. Lin, H. L. Xin and D. Wang, *J. Mater. Chem. A*, 2015, **3**, 22129–22135.

71 D. Zhang, F. Wu, M. Peng, X. Wang, D. Xia and G. Guo, *J. Am. Chem. Soc.*, 2015, **137**, 6263–6269.

72 J. Li, S. Sharma, X. Liu, Y.-T. Pan, J. S. Spendelow, M. Chi, Y. Jia, P. Zhang, D. A. Cullen, Z. Xi, H. Lin, Z. Yin, B. Shen, M. Muzzio, C. Yu, Y. S. Kim, A. A. Peterson, K. L. More, H. Zhu and S. Sun, *Joule*, 2019, **3**, 124–135.

73 Q. Li, L. Wu, G. Wu, D. Su, H. Lv, S. Zhang, W. Zhu, A. Casimir, H. Zhu, A. Mendoza-Garcia and S. Sun, *Nano Lett.*, 2015, **15**, 2468–2473.

74 J. Zhu, Y. Yang, L. Chen, W. Xiao, H. Liu, H. D. Abruña and D. Wang, *Chem. Mater.*, 2018, **30**, 5987–5995.

75 Q. Cheng, S. Yang, C. Fu, L. Zou, Z. Zou, Z. Jiang, J. Zhang and H. Yang, *Energy Environ. Sci.*, 2022, **15**, 278–286.

76 M. Nie, Z. Wang, D. He, W. Gan and Q. Yuan, *ACS Sustain. Chem. Eng.*, 2024,

12, 16700–16710.

77 X. Cao, H. Guo, Y. Han, M. Li, C. Shang, R. Zhao, Q. Huang, M. Li, Q. Zhang, F. Lv, H. Tan, Z. Qian, M. Luo and S. Guo, *Nat. Commun.*, 2025, **16**, 2851.

78 W.-J. Zeng, C. Wang, Q.-Q. Yan, P. Yin, L. Tong and H.-W. Liang, *Nat. Commun.*, 2022, **13**, 7654.

79 J. Lai, S. Chen, X. Liu, X. Yan, Z. Qin, L. Xie, Z. Lin, Z. Cai, Y. Zhao, H.-L. Wang, Y. Huang and Q. Li, *ACS Catal.*, 2023, **13**, 11996–12006.

80 X. Liu, Y. Wang, H. He, Z. Zhao, X. Luo, S. Zhang, G. Lu, D. Su, Y. Wang, Y. Huang and Q. Li, *Nat. Commun.*, 2025, **16**, 4895.

81 P. Kuang, Z. Ni, B. Zhu, Y. Lin and J. Yu, *Adv. Mater.*, 2023, **35**, 2303030.